



A comprehensive library of human transcription factors for cell fate engineering

Alex H. M. Ng^{1,2,3,14}, Parastoo Khoshakhlagh^{1,2,3,14}, Jesus Eduardo Rojo Arias^{4,13}, Giovanni Pasquini⁴, Kai Wang^{5,6}, Anka Swiersy⁴, Seth L. Shipman⁷, Evan Appleton^{1,2,3}, Kiavash Kiaee^{1,2,3}, Richie E. Kohman^{1,2}, Andyna Vernet², Matthew Dysart^{1,2}, Kathleen Leeper^{1,2}, Wren Saylor^{1,2}, Jeremy Y. Huang^{1,2}, Amanda Graveline², Jussi Taipale^{8,9,10}, David E. Hill^{1,11}, Marc Vidal^{1,11}, Juan M. Melero-Martin^{5,6}, Volker Busskamp^{10,12}✉ and George M. Church^{1,2,3}✉

Human pluripotent stem cells (hPSCs) offer an unprecedented opportunity to model diverse cell types and tissues. To enable systematic exploration of the programming landscape mediated by transcription factors (TFs), we present the Human TFome, a comprehensive library containing 1,564 TF genes and 1,732 TF splice isoforms. By screening the library in three hPSC lines, we discovered 290 TFs, including 241 that were previously unreported, that induce differentiation in 4 days without alteration of external soluble or biomechanical cues. We used four of the hits to program hPSCs into neurons, fibroblasts, oligodendrocytes and vascular endothelial-like cells that have molecular and functional similarity to primary cells. Our cell-autonomous approach enabled parallel programming of hPSCs into multiple cell types simultaneously. We also demonstrated orthogonal programming by including oligodendrocyte-inducible hPSCs with unmodified hPSCs to generate cerebral organoids, which expedited in situ myelination. Large-scale combinatorial screening of the Human TFome will complement other strategies for cell engineering based on developmental biology and computational systems biology.

A longstanding goal of stem cell, tissue and organoid engineering is the creation of any cell type or tissue in a facile, controlled manner. This is foundational for accurate cellular modeling in fundamental science, disease modeling, drug discovery and regenerative medicine. hPSCs have a virtually unlimited expansion capability and the potential to differentiate into any cell type. However, reliable protocols to generate most cell lineages are lacking, and existing protocols are often limited by long time scales or modest efficiencies. Many established protocols attempt to mimic the complexity of developmental biology, with its protracted timelines. During development, the process of cell-type specification is intertwined with other regulatory events that spatiotemporally position the proper cell types in defined population sizes but are not relevant to in vitro protocols that aim to rapidly generate large numbers of cells. Most current protocols also depend on external signals with known roles in development, such as soluble factors or mechanical cues, which often converge on TFs to control cell-type-specific genetic programs. This reliance on external cues, which are often incompatible among different specialized cell types, makes it challenging to generate multiple lineages in the same culture.

An alternative approach is direct activation of TFs, which can both shorten the time for cell conversion and isolate it from other developmental events. TF induction has been shown

to transdifferentiate cells between lineages¹, reprogram somatic cells to pluripotency² and differentiate stem cells³. Previous studies on applying TFs for cell fate engineering have used either experimental testing of a limited set of developmentally relevant TFs^{4–8} or computational prediction of TFs inferred from genome-scale datasets with modest accuracy^{9–11}. However, the field has lacked a global experimental study of the estimated 1,600 TFs in the human genome¹². The largest screen to our knowledge explored 481 TFs at once¹³.

After constructing the Human TFome, we screened each TF for its ability to induce differentiation of three human induced pluripotent stem cell (hiPSC) lines. Of the 290 hits, we found that 241 had not been previously associated with cell differentiation. We characterized four of the 290 TFs in depth—*ATOH1*, *NKX3-1*, *ETV2* and *SOX9*—which programmed hiPSCs within 4 days into induced neurons, induced fibroblasts, vascular endothelial-like cells and induced oligodendrocytes, respectively. We also demonstrated parallel programming of hiPSCs into two or three defined cell types simultaneously in the same culture without lineage-specific cues. Finally, we developed an orthogonal programming approach by including *SOX9*-engineered, oligodendrocyte-producing hiPSCs at the genesis of developmentally inspired cerebral organoids, which accelerated myelination.

¹Department of Genetics, Blavatnik Institute, Harvard Medical School, Boston, MA, USA. ²Wyss Institute for Biologically Inspired Engineering at Harvard University, Boston, MA, USA. ³GC Therapeutics, Inc, Cambridge, MA, USA. ⁴Technische Universität Dresden, Center for Molecular and Cellular Bioengineering (CMCB), Center for Regenerative Therapies Dresden (CRTD), Dresden, Germany. ⁵Department of Cardiac Surgery, Boston Children's Hospital, Boston, MA, USA. ⁶Department of Surgery, Harvard Medical School, Boston, MA, USA. ⁷Gladstone Institutes and University of California, San Francisco, San Francisco, CA, USA. ⁸Department of Biochemistry, University of Cambridge, Cambridge, UK. ⁹Department of Medical Biochemistry and Biophysics, Karolinska Institute, Stockholm, Sweden. ¹⁰Applied Tumor Genomics Program, Faculty of Medicine, University of Helsinki, Helsinki, Finland. ¹¹Center for Cancer Systems Biology (CCSB), Dana-Farber Cancer Institute, Boston, MA, USA. ¹²Department of Ophthalmology, Medical Faculty, University of Bonn, Bonn, Germany. ¹³Present address: Wellcome-MRC Cambridge Stem Cell Institute, Jeffrey Cheah Biomedical Centre, Cambridge Biomedical Campus, University of Cambridge, Cambridge, UK. ¹⁴These authors contributed equally: Alex H. M. Ng, Parastoo Khoshakhlagh.

✉e-mail: volker.busskamp@ukbonn.de; gchurch@genetics.med.harvard.edu

Results

290 TFs individually induce stem cell differentiation. We generated a library containing 1,564 human TFs, including 1,732 splice-isoform-level open reading frames (ORFs) (Supplementary Fig. 1a,b, Supplementary Table 1 and Methods), annotated based on a rigorous curation¹⁴. Cloning from complementary DNA (cDNA) is a bottleneck in generating ORF collections owing to low or tissue-confined TF expression in the source material. We overcame this by de novo synthesis of the 273 ORFs that were not available in existing large ORF collections^{15–18} (Supplementary Fig. 1c) and merged them to create the Human TFome.

To express the Human TFome in hiPSCs, we first cloned the library as one pool into an all-in-one doxycycline-inducible (Tet-On), puromycin-selectable lentiviral vector (Supplementary Fig. 1d–h). We ensured that cells received, at most, one TF by transducing them with the pooled library at a low multiplicity of infection (MOI) of 0.1, and we confirmed the induction of TF overexpression (Supplementary Fig. 1i). We transduced, in triplicates, three hiPSC lines (PGP1, CRTD5 and ATCC-DYS0100) that have similar characteristics (that is, all reprogrammed from male fibroblasts using Sendai virus) to reduce effects arising from the variability among hiPSC lines. Greater than 87% TF coverage was achieved in all three hiPSC lines (Supplementary Fig. 1j) by transducing a sufficient number of cells.

We used loss of pluripotency as a readout and enriched two cell populations by fluorescence-activated cell sorting (FACS): 1) ‘differentiated’ cells, which we define here as cells that have downregulated expression of pluripotency markers but have not been evaluated for expression of cell-type-specific markers and 2) cells that remained pluripotent (Fig. 1a and Supplementary Fig. 2a). Four days post TF induction (dpi), we stained cells for the pluripotency marker TRA-1-60 (refs. ^{19,20}) and sorted for differentiated cells (low TRA-1-60 signal) and pluripotent cells (high TRA-1-60 signal) (Supplementary Fig. 2b,c). To identify TFs enriched in the two populations, we amplified the integrated TFs using universal primers for Illumina sequencing and sequenced them. A score threshold defined by the ratio of TF counts in TRA-1-60 low versus high gates was used to identify TFs responsible for differentiation (Supplementary Fig. 2d and Methods).

Our screen identified 290 TFs that individually induced differentiation in at least two hiPSC lines and 65 TFs in all three lines (Fig. 1b, Supplementary Fig. 2e and Supplementary Tables 2 and 3), despite the variability among hiPSC lines^{21,22}. A PubMed query indicated that 241 of the 290 TFs (83.1%) and 54 of the 65 TFs (83.0%) have not been previously reported as programming or differentiation factors upon overexpression (Fig. 1b and Supplementary Table 4). The hits included known differentiation-inducing TFs, such as *NEUROG1* (ref. ²⁰) and *ASCL1* (ref. ²³), confirming the biological relevance of our screen. For validation, we selected the top TFs in each of the four overlapping groups of hits from the three lines (Supplementary Fig. 2e), for a total of 16 TFs. For screening, we used lentiviruses owing to their highly titratable transduction, which enabled us to perform a controlled Human TFome screen at a single copy per cell. However, to validate individual TFs, we used PiggyBac transposons, both to avoid the multi-step lentiviral production, which impedes high-throughput cell line engineering, and to reduce the silencing and variable expression associated with lentiviral vectors. Indeed, we observed increased differentiation efficiency using PiggyBac compared to lentivirus for a positive-control TF, *NEUROG1* (Fig. 1c). All 16 TFs were successfully validated in the PiggyBac system based on the loss of *NANOG*, *OCT4/POU5F1* or *SOX2* expression at 4 dpi (Fig. 1d and Supplementary Fig. 2f).

Next, we characterized the identity and functionality of the differentiated cells induced by four TFs: *ATOH1*, *NKX3-1*, *ETV2* and *SOX9*.

***ATOH1* programs hiPSCs into induced neurons.** *ATOH1* was the most efficient driver of differentiation in all three hiPSC lines (Fig. 1d). This TF has been implicated in the development of inner ear hair cells²⁴. It has also been used to induce neuronal differentiation in stem cells in conjunction with soluble neurogenesis cues and culturing techniques^{25,26}. We tested whether *ATOH1* alone is sufficient to program hiPSCs into induced neurons without specialized culturing conditions. Indeed, we observed rapid 4-day neuronal programming without changing the media composition, as $99 \pm 1\%$ of *ATOH1*-induced cells were positive for the neuronal marker NCAM (Fig. 2a), and cells exhibited neuronal morphology based on TUBB3 (Fig. 2b) and NF200 protein expression (Supplementary Fig. 3a). *ATOH1*-programmed cells and primary neurons were transcriptomically similar based on unbiased principal component analysis (PCA) (Fig. 2c) and upregulation of key neuronal genes (Fig. 2d and Supplementary Table 5). This was corroborated by CellNet network-based transcriptomic analysis (Supplementary Fig. 3b) and by the enrichment of neuronal gene ontologies in the upregulated genes (Supplementary Fig. 3c). Furthermore, the downregulation of pluripotency genes was confirmed transcriptionally (Supplementary Fig. 3d). We categorized these cells as ‘induced’, which we define here as cells with concurrent expression of functional markers of a specific lineage and residual levels of pluripotency markers.

To assess the function of the induced neurons, after 4 dpi, we cultured them without further doxycycline administration in neuronal maturation media and performed whole-cell patch-clamp electrophysiology. We observed single action potentials in response to current injection at 7 dpi (Supplementary Fig. 3e), trains of action potentials at 14 dpi (Fig. 2e) and spontaneous action potentials at 21 dpi (Supplementary Fig. 3f; summarized in Fig. 2f). Altogether, these results show that *ATOH1* alone can program hiPSCs into induced neurons that remain functional in long-term cultures.

***NKX3-1* programs hiPSCs into induced fibroblasts.** *NKX3-1* was the second most efficient hit from our validation studies (Fig. 1d). This TF is essential in prostate differentiation²⁷ and can replace *OCT4/POU5F1* in fibroblast reprogramming into iPSCs²⁸. However, *NKX3-1* has not been reported for hPSC differentiation. We used CellNet²⁹ to ascertain the identity of *NKX3-1*-induced cells based on transcriptomic network analysis: *NKX3-1*-programmed cells were serendipitously identified as fibroblasts (Supplementary Fig. 4a).

We overexpressed *NKX3-1* in hiPSCs with no additional soluble differentiation cues. At 4 dpi, $79 \pm 2\%$ of the cells expressed the fibroblast marker VIM as revealed by flow cytometry (Fig. 2g and Supplementary Fig. 4b). *NKX3-1*-induced cells were also positive for ALCAM and HSP47 by immunostaining (Fig. 2h). The cells had a transcriptomic signature similar to that of primary fibroblasts based on unbiased PCA (Fig. 2i) and upregulation of key fibroblast genes as shown by RNA sequencing (RNA-seq) (Fig. 2j and Supplementary Table 5). Gene Ontology analysis showed upregulation of fibroblast-associated genes (Supplementary Fig. 4c) and downregulation of the pluripotency genes *NANOG* and *OCT4/POU5F1* (Supplementary Fig. 4d).

A hallmark of fibroblasts is their function in wound healing and their ability to remodel the extracellular matrix. These can be assessed in scratch³⁰ and collagen contraction assays³¹ in vitro. At 4 dpi, without switching to fibroblast-specific media and without further doxycycline administration, after we scratched the monolayer of *NKX3-1*-induced cells, the cells migrated to seal the wound, whereas non-induced cells did not (Fig. 2k,l). In a separate functional assay, collagen-embedded *NKX3-1*-induced cells were able to contract and reduce the surface area of the collagen gel (Supplementary Fig. 4e,f). Hence, our data demonstrated that *NKX3-1* alone is a potent driver of differentiation into induced fibroblasts, with functionality in vitro.

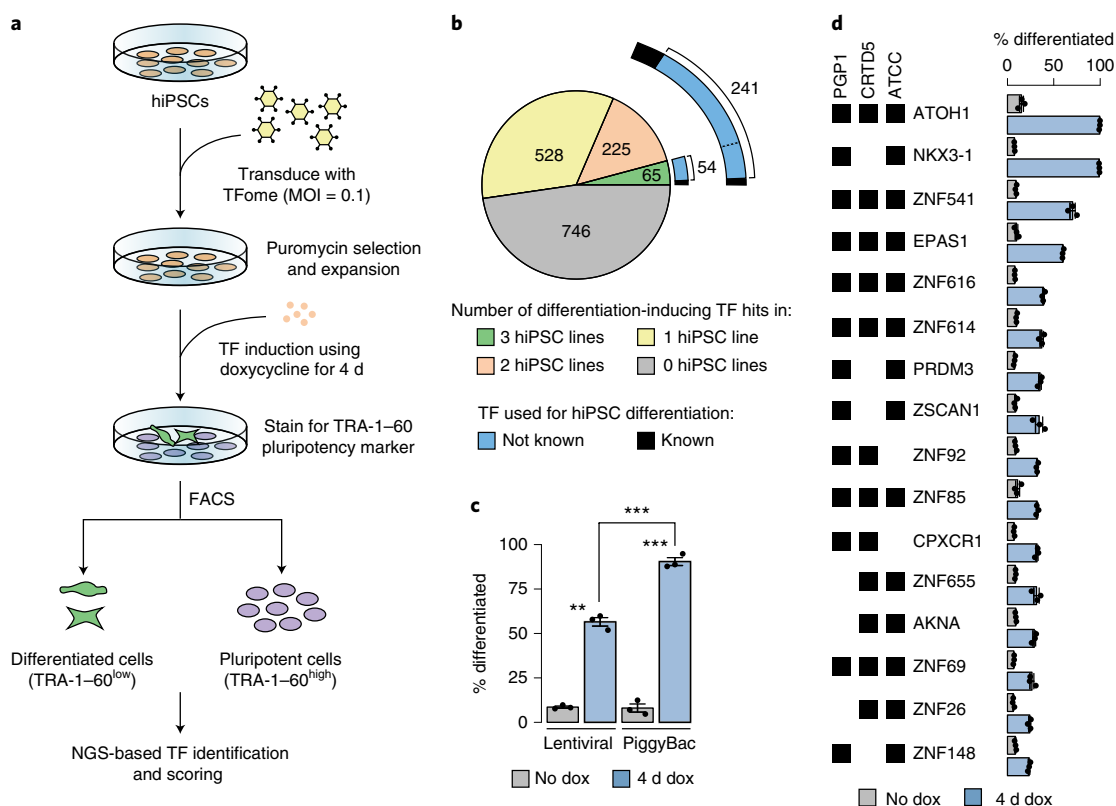


Fig. 1 | Creation of the Human TFome expression library and its application for cell fate engineering. **a**, Schematic of Human TFome screening for stem cell differentiation. MOI = 0.1 ensures single TF integration per cell. **b**, The Human TFome screen identifies previously unreported individual TFs that induce differentiation in multiple hiPSC lines. The pie chart shows the number of differentiation-inducing TF hits in 0, 1, 2 or 3 hiPSC lines. Donut charts show the number of TF hits previously known or not known to drive differentiation upon induction. **c**, Higher differentiation efficiency in PiggyBac-mediated versus lentiviral-mediated TF induction. Flow cytometry for differentiated cells based on loss of pluripotency markers at 4 dpi using *NEUROG1* as a canonical differentiation-inducing TF. Mean \pm s.e.m., $n=3$ biologically independent samples per group, two-sided Student's t -test. **d**, Validation of top TF hits in individual cell lines at 4 dpi. Percentage of differentiation was calculated by loss of pluripotency markers using flow cytometry. Mean \pm s.e.m., $n=3$ biologically independent samples per group, two-sided Student's t -test. * $P < 0.05$, ** $P < 0.01$, *** $P < 0.001$. Exact P values are provided in Supplementary Table 7. NGS, next-generation sequencing.

ETV2 isoform 2 programs hiPSCs into vascular endothelial-like cells. Our differentiation approach, which does not use lineage-specific media, might facilitate the generation of multiple cell types in the same culture. Given the importance of vascularization in building synthetic tissues, along with the indispensable role of *ETV2* in vascular differentiation from PSCs³², we aimed to determine *ETV2*'s programming ability without lineage-specific media. We queried *ETV2*'s rank in our screen, where it was among the top hits in one of the three hiPSC lines. As TF splice isoforms play important roles in cell differentiation³³, and only *ETV2* isoform 1 was included in the screen, we aimed to determine the effect of all four of *ETV2*'s annotated splice isoforms (Supplementary Fig. 5a) on cell-autonomous vascular cell conversion. The *ETV2* isoform used in a previous study for hiPSC differentiation³² could not be readily ascertained, and the contribution of these isoforms to vascular programming without lineage-specific media has not been examined.

We tested all four isoforms of *ETV2* independently and found that isoforms can have a major effect on programming efficiency. Using *ETV2* isoform 2 (ENST00000402764.6), $95 \pm 0.2\%$ of cells expressed the endothelial cell marker VE-cadherin (CDH5) at 4 dpi (Fig. 3a), compared to only $48 \pm 1\%$ using the longer *ETV2* isoform 1 (Fig. 3a). The other two isoforms had low to no ability to induce endothelial conversion (isoform 3: $21 \pm 2\%$ and isoform 4: $0 \pm 0\%$; Fig. 3a), despite similar integrated vector copy numbers for all four

isoforms (Supplementary Fig. 5b). Only isoform 2 induced nearly complete expression of VE-cadherin, with its characteristic cobblestone morphology (Fig. 3b). We examined the functionality of these four cell populations in angiogenesis assays. Only isoform 2 had high tubulogenesis capability (Fig. 3c).

We focused on *ETV2* isoform 2, the most potent splice variant, for deeper analysis. At 4 dpi, these cells had a transcriptomic signature similar to that of primary endothelial cells based on unbiased PCA (Fig. 3d), upregulation of key vascular endothelial genes (Fig. 3e and Supplementary Table 5) and a transcriptomic comparison of highly variable genes (Supplementary Fig. 5c). They also had an endothelial cell type classification based on CellNet network-based transcriptomic analysis (Supplementary Fig. 5d) and on Gene Ontology analysis of the upregulated genes (Supplementary Fig. 5e). Furthermore, we detected increased expression of *PLVAP*, *PECAM1* and *CDH5* (VE-cadherin) in *ETV2* isoform 2-induced cells, along with downregulation of pluripotency genes by single-cell RNA sequencing (scRNA-seq) (Fig. 3f). Downregulation of pluripotency genes was further confirmed by bulk RNA-seq (Supplementary Fig. 5f) and flow cytometry (Supplementary Fig. 5g). Although these cells expressed endothelial functional markers, they continued to express residual amounts of the pluripotency marker *OCT4* at day 4. We, therefore, defined them as 'vascular endothelial-like' cells. Notably, the cells remained stably programmed after the induction of exogenous *ETV2* isoform 2 was stopped (Supplementary Fig. 5h).

We assessed the angiogenic ability of the cells. Using an in vitro tube formation assay, we observed lumens by transmission electron microscopy (TEM) (Fig. 3g) with diameters of $4.3 \pm 0.7 \mu\text{m}$ (Fig. 3h) and tight junctions (Supplementary Fig. 5i), similar to that of capillaries in vivo³⁴. To assess function in vivo, we transplanted *ETV2*-induced cells subcutaneously into nude mice. Seven days after transplantation, we observed mature blood vessels derived from the cells, as evidenced by human-specific CD31-lined lumens supported by mouse α -smooth muscle actin (SMA)-positive perivascular cells (Fig. 3i). The blood vessels integrated with the host circulatory system and were perfused, as shown by the presence of host red blood cells within their lumens in a serial tissue section (Fig. 3j). We observed 40 ± 6 vessels per mm^2 on average (Fig. 3k).

Parallel cell programming in co-cultures. With the aim of constructing complex tissues, we investigated the concept of parallel programming. In this approach, multiple lineages are generated simultaneously in the same dish in lineage-independent media (Fig. 4a). We mixed inducible neuronal, endothelial and fibroblast hiPSCs in a pairwise fashion with identical ratios (that is, *ETV2* + *NKX3-1*, *ATOHI1* + *NKX3-1* and *ATOHI1* + *ETV2* hiPSCs) and activated TF expression for 4 d. The final cell populations were assessed by immunostaining. All three cell-type-specific markers—MAP2, ALCAM and VE-cadherin—were expressed in the co-cultures as expected (Fig. 4b). We quantified the populations by flow cytometry and observed similar outcomes, with approximately equal proportions of each cell type (Fig. 4c). These data suggest that cell types can be differentiated in parallel, in the same media and without additional soluble factors.

Next, we combined the three cell types, inducible *ATOHI1*, *NKX3-1* and *ETV2* hiPSCs, in one culture and induced differentiation. The resulting cells expressed markers for fibroblasts, neurons and vascular endothelial cells (Fig. 4b,c). The proportions of each cell type by flow cytometry were $15.9 \pm 0.6\%$ NCAM⁺, $22.6 \pm 1.1\%$ VIM⁺ and $38.1 \pm 1.6\%$ VE-cadherin⁺. We also performed scRNA-seq to assess whether the transcriptomic signatures of the three cell lineages were retained. Therefore, a more sensitive scRNA-seq method was desired rather than maximizing the number of cells analyzed. This was achieved using FACS-based single-cell isolation and Smart-seq2 library preparation, which detects more molecules per cell than microfluidic-based methods³⁵. We observed three distinct populations, with each one correlating to one induced TF (Fig. 4d). In each population, the TF matched its expected cell-type-specific expression signature based on unbiased marker selection because

some canonical genes showed weak expression and were not readily detected by scRNA-seq (Fig. 4e). We detected strong cell-type-specific transcriptomic signatures in the few cells that were captured. To test parallel programming in three-dimensional cell culture, we performed similar mixing experiments and generated spheroids. All three lineages appeared, as assessed by microscopy and flow cytometry (Supplementary Fig. 6a,b).

SOX9 programs hiPSCs into induced oligodendrocytes. Organoid technology is limited by the long timelines required for the emergence of certain cell types. In cerebral organoids, for instance, it takes 103–210 d for mature myelin to form^{36,37}. There are no reported protocols, to our knowledge, to differentiate hiPSCs to myelin-producing oligodendrocytes in lineage-independent media using TFs^{38,39}. To address this need with the Human TFome library, we identified 15 TFs involved in oligodendrocyte differentiation and maturation in vivo using prior knowledge from developmental biology (Supplementary Table 6). We queried their rank in our screen, which yielded *SOX9* as the top hit. *SOX* family members have broad roles in the development of various tissues^{40,41}, and *SOX9* has been used in combination with *NFIB* and soluble factors to induce astrocyte differentiation⁴². However, *SOX9* has not been reported, individually or in a combination, to program hPSCs into oligodendrocytes.

At day 4 after *SOX9* induction, hiPSCs were converted to oligodendrocyte progenitors without additional lineage-specifying cues (Fig. 5a). The cells expressed the hallmark oligodendrocyte progenitor marker O4 ($82 \pm 6\%$) and were positive for NG2, a glial progenitor marker, by immunostaining (Fig. 5b). Their transcriptomic signatures were similar to primary oligodendrocytes based on unbiased PCA (Fig. 5c), upregulation of key oligodendrocyte genes (Fig. 5d and Supplementary Table 5) and transcriptomic comparison of highly variable genes (Supplementary Fig. 7a). We also detected expression of the oligodendrocyte lineage markers *CSPG4* (NG2) and *MYRF* by scRNA-seq (Fig. 5e). Pluripotency genes were downregulated in both scRNA-seq (Fig. 5e) and bulk RNA-seq (Supplementary Fig. 7b).

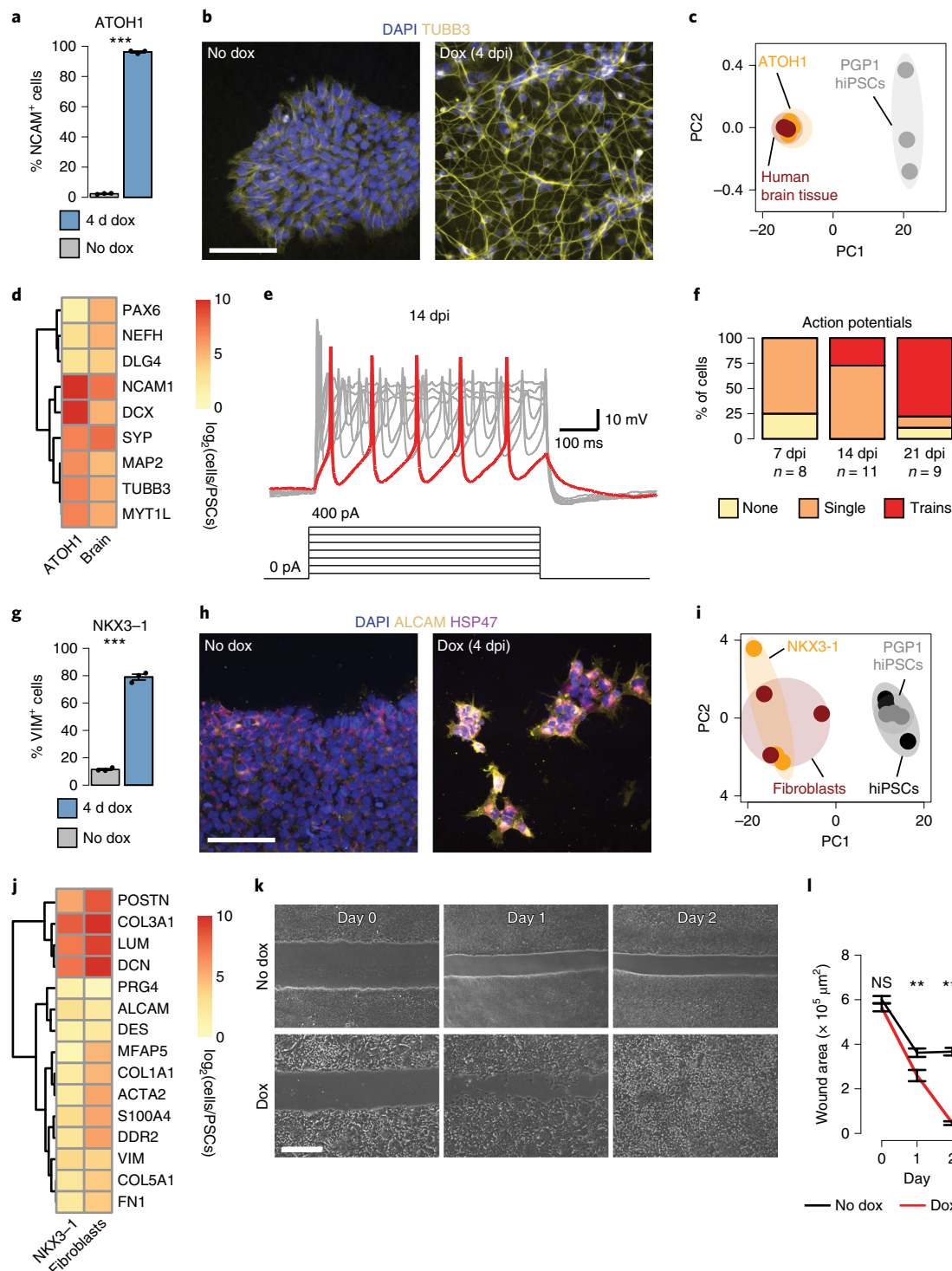
To assess the myelination potential of *SOX9*-induced cells, we applied parallel programming to produce an oligo-neuronal co-culture. We combined inducible *SOX9* hiPSCs along with our previously described, fully characterized hiPSC-derived inducible neurons, which project long axons upon differentiation²⁰. We then activated TF expression. At 3 dpi, without additional external culture-specific factors, we observed oligodendrocytes contacting

Fig. 2 | *ATOHI1* induces neurons and *NKX3-1* induces fibroblasts in lineage-independent media. **a**, *ATOHI1* drives hiPSCs into $99 \pm 1\%$ NCAM⁺ neurons at 4 dpi. Bar plot of flow cytometry for NCAM neuronal marker compared to non-induced cells. Mean \pm s.e.m., $n = 3$ biologically independent samples per group, two-sided Student's *t*-test. **b**, *ATOHI1*-induced cells exhibit neuronal morphology with TUBB3 neuronal protein marker expression at 4 dpi compared to non-induced cells using immunofluorescent staining. Scale bar, 100 μm . Experiments were performed independently at least three times with similar results. **c**, *ATOHI1*-induced cells are transcriptomically similar to human brain tissue. PCA of RNA-seq samples from *ATOHI1*-induced cells (orange) overlap with samples from human brain tissue (red) and are distinctly separated from PGP1 hiPSCs (gray). **d**, *ATOHI1*-induced cells show similar upregulation of neuronal markers as human brain tissue. Heat map of neuronal gene expression profiles. **e**, *ATOHI1*-induced cells are electrophysiologically functional at 14 dpi. Electrophysiology recordings by whole-cell patch clamping after current injection. **f**, *ATOHI1*-induced cells mature over time to exhibit spontaneous trains of action potentials. Bar plots of percentage of cells having each type of action potential at 7, 14 and 21 dpi. $n =$ number of single cells. **g**, *NKX3-1* rapidly and efficiently induces hiPSCs into fibroblasts. Bar plot of flow cytometry for VIM fibroblast marker at 4 dpi compared to non-induced cells. Mean \pm s.e.m., $n = 3$ biologically independent samples per group, two-sided Student's *t*-test. **h**, *NKX3-1*-induced cells show fibroblast morphology with ALCAM and HSP47 fibroblast protein marker expression at 4 dpi using immunofluorescent staining. Scale bar, 100 μm . Experiments were performed independently at least three times with similar results. **i**, *NKX3-1*-induced cells are transcriptomically similar to primary fibroblasts. PCA of RNA-seq samples from *NKX3-1*-induced cells (orange) overlap with samples from primary fibroblasts (red), with a clear distance away from PGP1 hiPSCs (gray). **j**, *NKX3-1*-induced cells show similar upregulation of fibroblast markers as primary fibroblast based on RNA-seq analysis. Heat map of fibroblast gene expression profiles. **k**, *NKX3-1*-induced cells exhibit functionality in an in vitro wound healing assay by repairing a scratch in a confluent cell monolayer. Bright-field images of 4-dpi *NKX3-1*-induced cells at days 0, 1 or 2 after gap creation. Scale bar, 100 μm . Experiments were performed independently at least three times with similar results. **l**, Significant reduction in wound area by *NKX3-1*-induced cells (red) but not hiPSCs (black). Quantification of wound area in scratch assay. Mean \pm s.e.m., $n = 3$ biologically independent samples per group, two-sided Student's *t*-test. ****** $P < 0.01$ and ******* $P < 0.001$. Exact *P* values are provided in Supplementary Table 7. NS, not significant.

axons and beginning the ensheathment process (Supplementary Fig. 7c). Robust myelin sheaths around axons were visualized by TEM after 30 d of co-culture in photo-micropatterned microchannels^{43,44} (Fig. 5f). We computed G-ratios, a metric for compact myelin, to be 0.56 ± 0.02 (Fig. 5g), which are similar to those of the human brain ($0.5\text{--}0.8$)⁴⁵. These results confirmed the *in vitro* myelination functionality of SOX9-induced oligodendrocytes.

To evaluate the *in vivo* engraftability and functionality of SOX9-induced oligodendrocytes, we transplanted the cells using established methods^{39,46} into Shiverer mice. This congenitally

hypomyelinated mouse model has a knockout in the myelin basic protein (*MBP*) gene. We detected engraftment of SOX9-induced cells in immunostained brain sections 10 weeks after transplantation based on the presence of MBP (Fig. 5h), which can be expressed only in the donor cells. No MBP was observed in the control group. Furthermore, based on TEM of brain cross-sections, we observed compact myelin in mice transplanted with SOX9-induced cells but rarely in the control group (Fig. 5i). The number of myelinated axons in mice transplanted with cells was significantly higher than in the control group (Fig. 5j; $P < 3.1 \times 10^{-5}$).



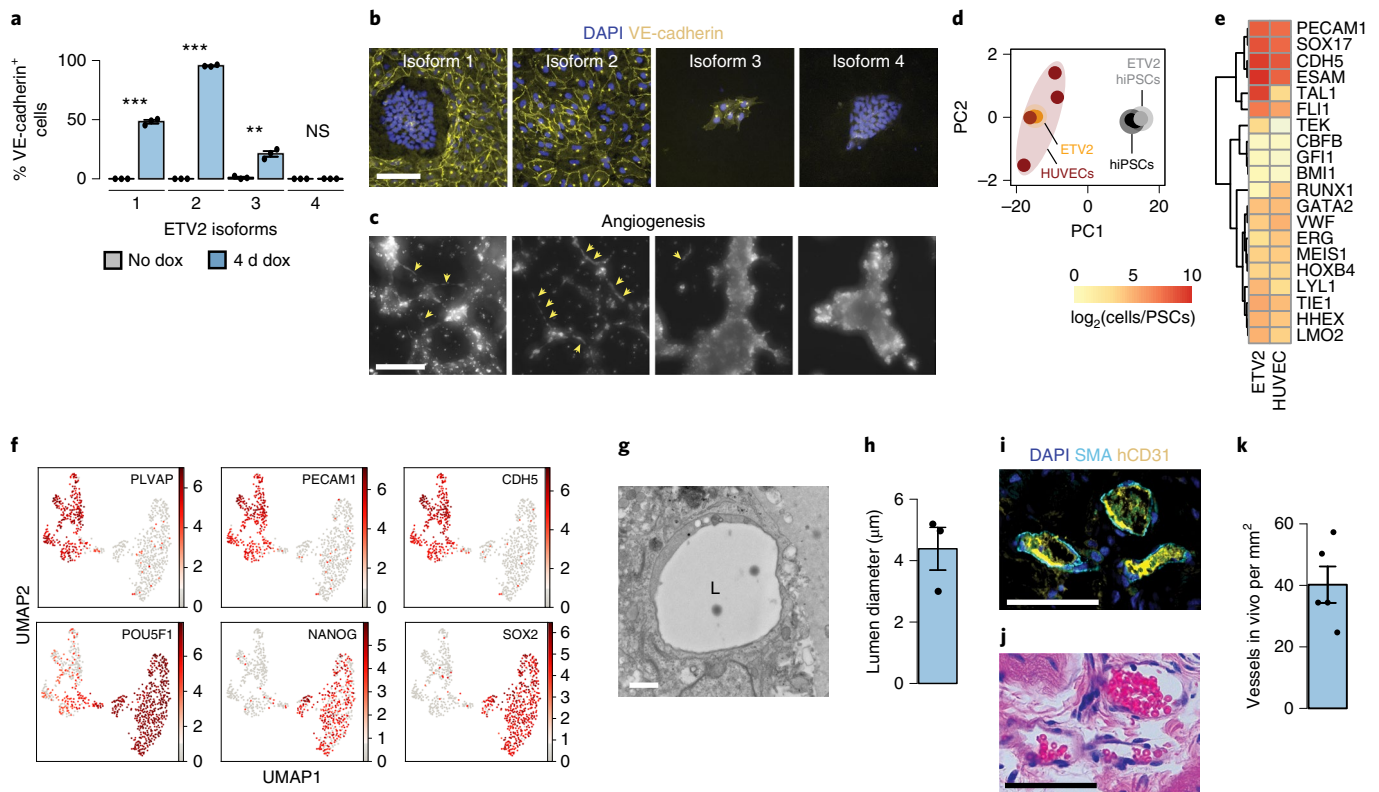


Fig. 3 | ETV2 isoform 2 induces vascular endothelial-like cells that form perfusable blood vessels in vivo. **a**, ETV2 isoform 2 induction differentiated hiPSCs into $95 \pm 0.2\%$ VE-cadherin⁺ (CDH5) vascular endothelial-like cells, which is superior to other splice isoforms. Bar plot of flow cytometry for VE-cadherin vascular endothelial marker at 4 dpi compared to non-induced cells for each splice isoform. Mean \pm s.e.m., $n = 3$ biologically independent samples per group, two-sided Student's t -test. **b**, ETV2 isoform 2-induced cells exhibit homogeneous cobblestone endothelial morphology and VE-cadherin protein marker expression at 4 dpi compared to other splice isoforms and non-induced cells using immunofluorescent staining. Scale bar, 100 μm. Experiments were performed independently at least three times with similar results. **c**, 4-dpi ETV2 isoform 2-induced cells form angiogenic tubes overnight, marked by arrowheads. Fluorescence imaging of ETV2-induced cells on thick Matrigel. Scale bar, 300 μm. Experiments were performed independently at least three times with similar results. **d**, ETV2 isoform 2-induced cells are transcriptomically similar to primary HUVECs. PCA analysis of RNA-seq samples from ETV2 isoform 2-induced cells (orange) overlap with HUVECs (red) and are distinctly apart from PGP1 hiPSCs (gray) and HUVEC reference hiPSCs (black). **e**, ETV2 isoform 2-induced cells show similar upregulation of endothelial markers as HUVECs. Heat map of endothelial gene expression profiles. **f**, ETV2 isoform 2-induced cells homogeneously express vascular endothelial markers and lose pluripotency markers. Uniform manifold approximation and projection (UMAP) plot of scRNA-seq samples of ETV2 isoform 2-induced cells 4 dpi (left cluster) and hiPSCs (right cluster) showing gray (low) to red (high) for the level of gene expression of the indicated endothelial markers *PLVAP*, *PECAM1* and *CDH5* (VE-cadherin) and pluripotency markers *POU5F1/OCT4*, *NANOG* and *SOX2*, log₂ normalized. **g**, 4-dpi ETV2 isoform 2-induced cells form open lumens in an angiogenesis assay overnight. TEM on a cross-section of angiogenic tubes. Scale bar, 1 μm. Experiments were performed independently at least three times with similar results. **h**, Open lumens formed by ETV2 isoform 2-induced cells have diameters similar to capillaries. Quantification of lumen diameter. Mean \pm s.e.m., $n = 3$ biologically independent samples. **i**, ETV2 isoform 2-induced cells transplanted subcutaneously into nude mice form mature blood vessels in vivo. Immunofluorescent staining of a tissue section from the graft for the human-specific CD31 (hCD31) vascular endothelial protein marker shows human endothelial cells lining open lumens, which are mature based on the surrounding SMA⁺ pericytes. Scale bar, 50 μm. Experiments were performed independently at least three times with similar results. **j**, Blood vessels formed in vivo by ETV2 isoform 2-induced cells are perfused and integrated with the host circulatory system. Hematoxylin and eosin (H&E) staining of a tissue section (serial section from **i**) shows mouse red blood cells within the capillaries. Scale bar, 50 μm. Experiments were performed independently at least three times with similar results. **k**, Capillaries formed in vivo by transplanted ETV2 isoform 2-induced cells have similar density to in vivo tissues. Quantification of the number of hCD31⁺ blood vessels. Mean \pm s.e.m., $n = 5$ animals. ** $P < 0.01$, *** $P < 0.001$. Exact P values are provided in Supplementary Table 7. L, lumen; NS, not significant.

Taken together, our results demonstrate that induction of *SOX9* alone was sufficient to program hiPSCs cell autonomously into induced oligodendrocytes. The molecular profiles of the cells with continuous doxycycline administration were similar to those of primary oligodendrocytes, and the cells could form compact myelin in a co-culture and in hypomyelinated mice.

Orthogonal programming accelerates the myelination of cerebral organoids. To accelerate myelination in cerebral organoids and construct more accurate models of human brain tissue, we harnessed the *SOX9*-induced oligodendrocytes to introduce the

concept of orthogonal cell programming (Fig. 5k). In this approach, cell-autonomous TF overexpression is used in conjunction with a differentiation method that uses external cues (Supplementary Fig. 7d). To this end, we combined inducible *SOX9* hiPSCs with unmodified hiPSCs and induced cerebral organoid formation⁴⁷. After 4 d, we added doxycycline to induce *SOX9* expression in the orthogonally programmed group and compared it with the control group where *SOX9* was not induced. At 40 dpi, we observed myelin oligodendrocyte glycoprotein (MOG) in immunostained cross-sections of orthogonally programmed organoids (Fig. 5l) but not in the controls. TEM on these cross-sections showed robust

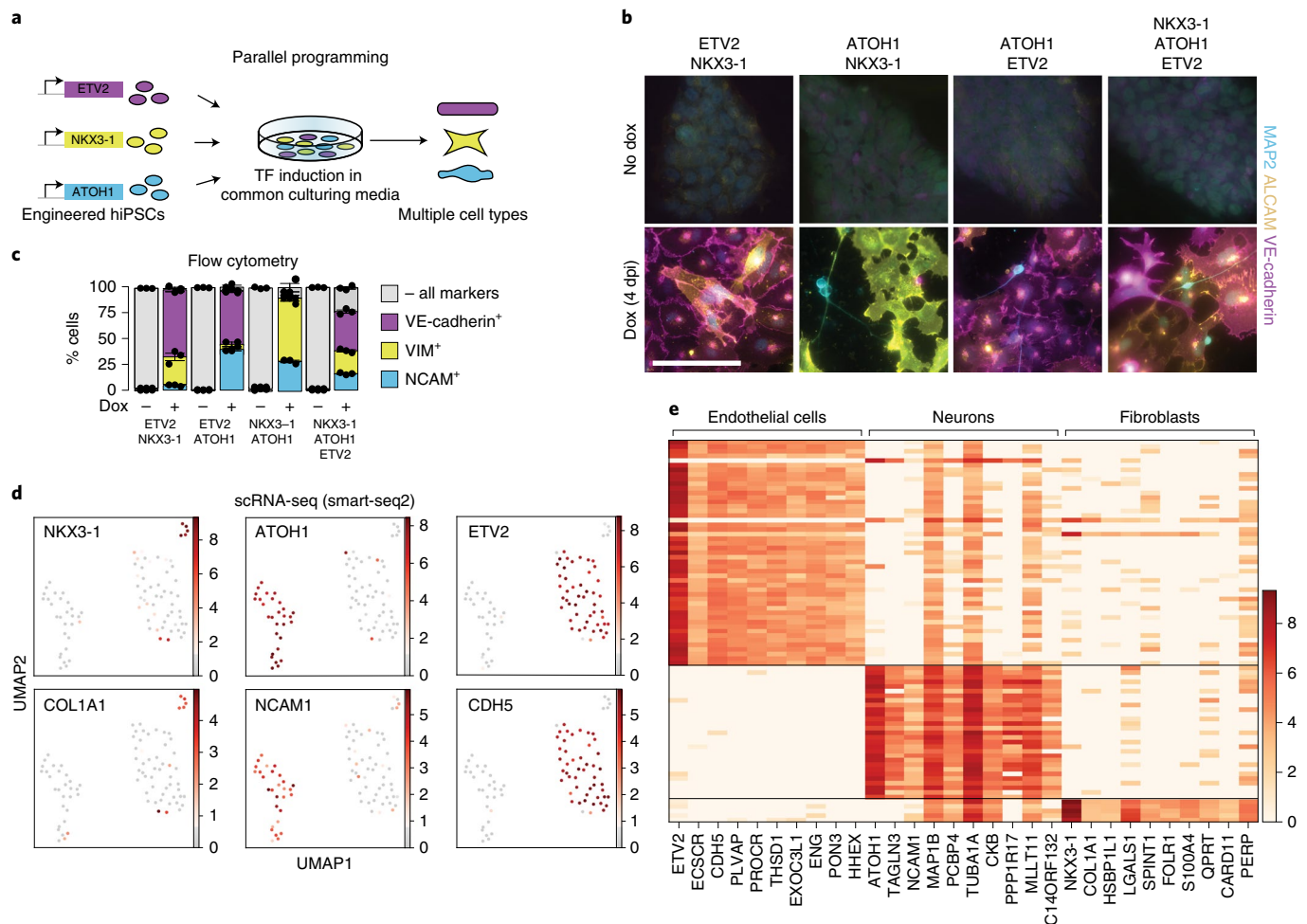


Fig. 4 | Parallel programming enables simultaneous differentiation of multiple cell types in the same dish. **a**, Schematic of parallel programming where TFs are induced and multiple cell types are produced in the same culture. **b**, Parallel programming enables induced neurons, fibroblasts and vascular endothelial-like cells to co-differentiate in the same culture and conditions. Engineered hiPSC lines co-cultured in a pairwise fashion or all together, 4 dpi or without induction, were immunofluorescently stained for the MAP2 neuronal marker, the ALCAM fibroblast marker and the VE-cadherin (CDH5) endothelial marker. Scale bar, 100 μ m. Experiments were performed independently at least three times with similar results. **c**, Parallel programming of cell lines mixed at equal ratios gives rise to co-cultures with similar proportions for each cell type at 4 dpi. Bar plot of flow cytometry for the VE-cadherin vascular endothelial marker, VIM fibroblast marker and NCAM neuronal marker at 4 dpi compared to non-induced cells. Mean \pm s.e.m., $n=3$ biologically independent samples per group. **d**, Triple parallel programmed co-cultures containing *ATOH1*-, *ETV2* isoform 2- and *NKX3-1*-induced cells 4 dpi homogeneously express the expected cell-type-specific markers. UMAP plot of scRNA-seq using Smart-seq2 library preparation shows three distinct populations. *NKX3-1*-induced cells express the *COL1A1* fibroblast marker; *ATOH1*-induced cells express the *NCAM1* neuronal marker; and *ETV2*-induced cells express the *CDH5* (VE-cadherin) endothelial marker. Color scale from gray (low) to red (high) shows the expression level of the indicated genes, log transformed. **e**, Triple parallel programmed cells show distinct transcriptomic signatures that correspond to expected cell-type-specific markers. Heat map of scRNA-seq showing the top ten marker genes from each cluster as computed by Student's *t*-test, log transformed expression. Single cells are presented as rows, and genes are presented as columns.

compact myelin formation in orthogonally programmed organoids (Fig. 5m), confirming that incorporation of SOX9-induced oligodendrocytes accelerated myelin maturation. The G-ratio of the myelinated axons was computed to be 0.52 ± 0.04 (Fig. 5n), which is similar to that of healthy human brains⁴⁵.

Discussion

The Human TFome enables systematic investigation of TF-based programming for cell engineering. We conducted a cell-type-agnostic screen of the complete library in three hiPSC lines using downregulation of the pluripotency marker TRA-1-60 as a readout. The screen revealed a more widespread ability of individual TFs to induce differentiation than anticipated, with 290 hits in at least two lines and 65 in all three lines. Our PubMed search indicated that

only 49 of the 290 hits have been previously associated with lineage programming, and, thus, 241 hits have not been reported previously. The cell conversions were rapid (4 d), efficient and induced by single TFs in mTeSR1 medium, without any alteration of soluble factors or mechanical cues.

Of the hits, we discovered four that differentiated hiPSCs into induced neurons, fibroblasts, oligodendrocytes and vascular endothelial-like cells. To our knowledge, other than work from our laboratories, current protocols for these cell types^{25,38,39,48–51} require cell-type-specific media components for the initiation of differentiation, even if TFs are also used. The *ATOH1*-induced neurons are similar to those described in our previous work, which were generated using TFs of the *Neurogenin* family²⁰, in that they do not require neuronal-induction culturing conditions, which is a major

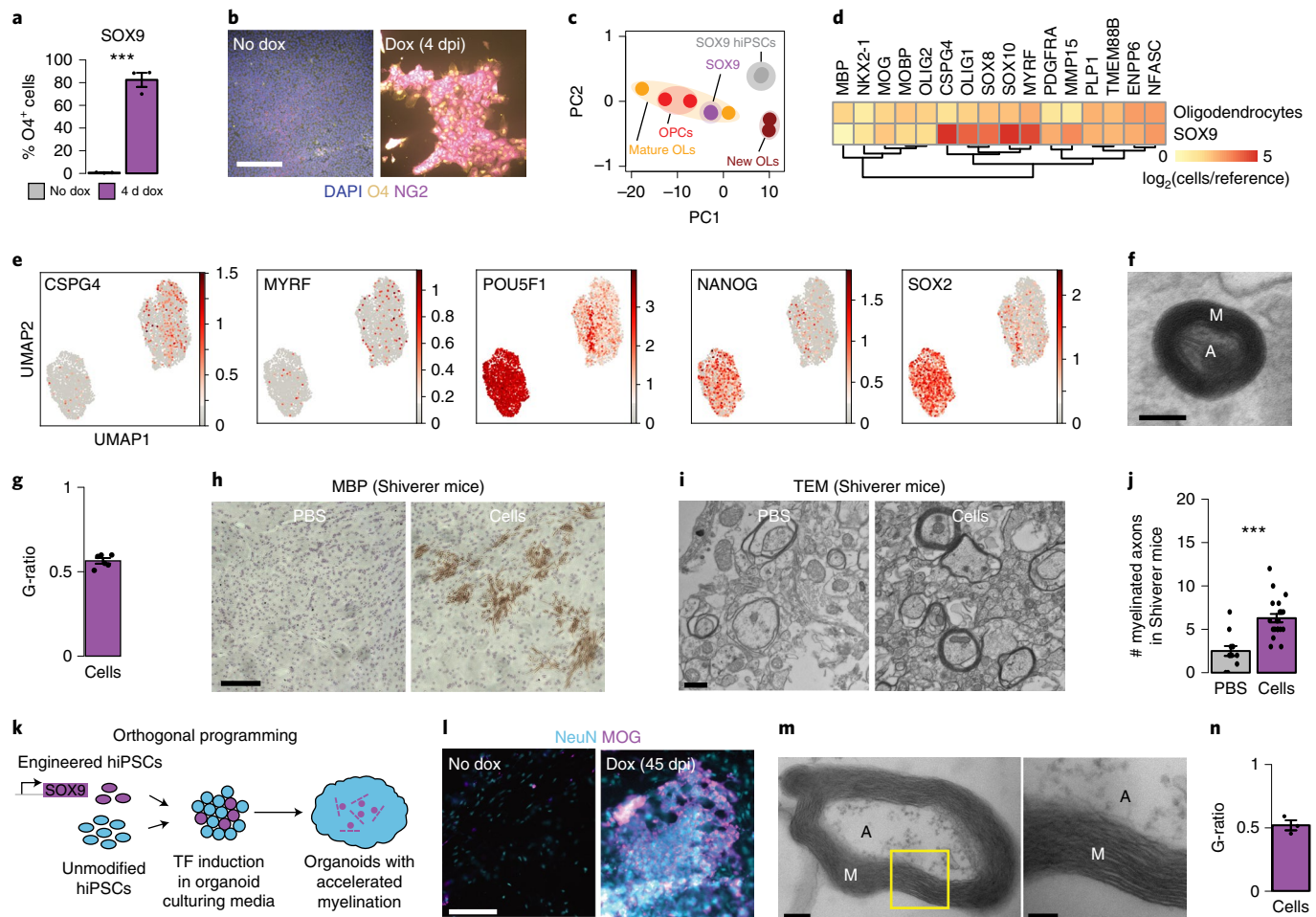


Fig. 5 | SOX9 induces oligodendrocytes that engraft and form compact myelin in vivo and in cerebral organoids. **a**, SOX9 rapidly and efficiently programs hiPSCs into induced oligodendrocytes at 4 dpi. Bar plot of flow cytometry for O4 oligodendrocyte marker compared to non-induced cells. Mean \pm s.e.m., $n=3$ biologically independent samples per group, two-sided Student's t -test. *** $P < 0.001$. **b**, SOX9-induced cells exhibit O4 and NG2 oligodendrocyte protein marker expression at 4 dpi compared to non-induced cells using immunofluorescent staining. Scale bar, 100 μ m. Experiments were performed independently at least three times with similar results. **c**, SOX9-induced cells are transcriptomically similar to primary oligodendrocytes. PCA of RNA-seq samples from SOX9-induced cells (purple) overlap with samples from primary mature oligodendrocytes (OLs; orange), with similarity to oligodendrocyte progenitor cells (OPCs; red) and are distinctly separated from newly formed oligodendrocytes (OLs; brown) and PGP1 hiPSCs (gray). **d**, SOX9-induced cells show similar upregulation of oligodendrocyte markers as primary oligodendrocytes. Heat map of oligodendrocyte gene expression profiles. **e**, SOX9-induced cells form a homogeneous cluster that expresses oligodendrocyte markers and loses pluripotency markers. UMAP plot of scRNA-seq samples of SOX9-induced cells 4 dpi (right cluster) and hiPSCs (left cluster) showing gray (low) to red (high) for the level of gene expression of the indicated oligodendrocyte markers *CSPG4* (NG2) and *MYRF* and pluripotency markers *POU5F1/OCT4*, *NANOG* and *SOX2*, \log_2 normalized. **f**, Parallel programming of SOX9-induced oligodendrocytes and hiPSC-derived neurons produces synthetic oligo-neuronal co-cultures that form compact myelin in vitro. TEM on a cross-section of the oligo-neuronal co-culture in the photo-micropatterned microchannels. Scale bar, 100 nm. Experiments were performed independently at least three times with similar results. **g**, Quantification of G-ratio for compact myelin is within the physiological range. Mean \pm s.e.m., $n=6$ independent samples. **h**, Transplanted SOX9-induced cells engraft and express MBP in Shiverer (*MBP* knockout) mice at 2.5 months. Immunofluorescent staining of a brain tissue section for the MBP myelin marker after PBS injection or SOX9-induced cell transplantation into Shiverer mice. Scale bar, 200 μ m. Experiments were performed independently at least three times with similar results. **i**, Transplanted SOX9-induced cells form compact myelin in Shiverer mice. TEM of a cross-section from Shiverer mice after PBS injection or SOX9-induced cell transplantation. Scale bar, 600 nm. Experiments were performed independently at least three times with similar results. **j**, Shiverer mice with transplanted SOX9-induced cells have significantly more myelinated axons than PBS-injected animals. Quantification of the number of myelinated axons from Shiverer mice after PBS injection or SOX9-induced cell transplantation. Mean \pm s.e.m., $n=12$ micrographs taken at distinct locations derived from two PBS-injected animals; $n=21$ micrographs taken at distinct locations derived from three animals with cell transplantation, two-sided Student's t -test. *** $P < 0.001$. Exact P values are provided in Supplementary Table 7. **k**, Schematic of orthogonal programming where engineered hiPSCs for TF-inducible differentiation are incorporated at the genesis of developmentally inspired cerebral organoids to synthetically accelerate myelination. **l**, Orthogonal programming of inducible SOX9 cells within cerebral organoids accelerated expression of the MOG myelin marker. Immunofluorescent staining of a cerebral organoid section for MOG myelin marker and NeuN neuronal marker in orthogonally induced versus non-induced organoids. Scale bar, 100 μ m. Experiments were performed independently at least three times with similar results. **m**, SOX9 orthogonally programmed organoids for compact myelin. TEM of myelin in a cerebral organoid. Yellow region magnified on the right. Scale bar, 200 nm. Inset scale bar, 100 nm. Experiments were performed independently at least three times with similar results. **n**, Quantification of G-ratio for compact myelin in cerebral organoids shows physiological resemblance. Mean \pm s.e.m., $n=3$ biologically independent samples. *** $P < 0.001$. Exact P values are provided in Supplementary Table 7. A, axon; M, myelin.

advantage. Our *NKX3-1*-induced fibroblast protocol represents an advance in that no TF-based differentiation protocol for fibroblasts has been reported, and current differentiation methods require embryoid body formation, collagen embedding and replating over 3 weeks of culture with unknown conversion efficiency⁴⁸. Our *ETV2* isoform 2 protocol for vascular endothelial-like cells generates 95% VE-cadherin⁺ cells compared to ~40% in previous work^{49–51}, emphasizing the importance of isoforms in cell programming. Our *SOX9*-induced oligodendrocyte protocol is more streamlined and facile than a previous TF-based method³⁸, which required multi-step, cell-type-specific media conditions to bring hiPSCs to the neural progenitor stage, followed by glial-specific soluble factors to promote oligodendrocyte differentiation.

We found that PiggyBac transposons, which were optimized for high-throughput individual cell line engineering, significantly improved differentiation efficiency compared to lentiviral gene transfer. We demonstrated that long-term TF induction is not required to differentiate cells into a stable cell fate. *ATOH1*-induced neurons and *NKX3-1*-induced fibroblasts were functional in vitro (Fig. 2e,f,k,l), and *ETV2*-induced vascular endothelial-like cells were functional in vivo (Fig. 3i–k) without continuous TF induction. The practical benefit is the alleviation of long-term replenishment of TF-induction molecules to achieve differentiation and the possibility of excising PiggyBac transposons from the genomes of engineered cells⁵².

A major challenge in tissue engineering is the generation of multiple cell types in one culture, especially supporting cells such as fibroblasts or endothelial cells⁵³. We showed that our lineage-independent differentiation approach can help address this issue. Previously, liver bud-like tissues containing multiple lineages were produced through heterogeneous expression of *Gata6* in hiPSCs in the same culture⁵⁴. However, control over cell identities and the ratios of each cell type were not attained owing to the lack of genetic switches to tune these parameters. Parallel programming using TFs discovered from our screen allowed us to achieve high-resolution control over cell-type composition and proportion. This enabled co-differentiation of hiPSCs into induced neurons, fibroblasts and vascular endothelial-like cells without lineage-specific cues. We also used parallel programming of induced oligodendrocytes and neurons to rapidly construct robust in vitro myelination models, featuring physiological cell–cell interactions.

Further research is needed to understand how cell types differentiated in parallel compare with homogeneously differentiated cells. Although our four protocols could override pluripotency networks to achieve nearly complete differentiation in 4 d, the resulting cells were not transcriptomically equivalent to their primary cell counterparts, despite having the expected functionality. We have also not explored whether our approach can mitigate the effects of different media compositions or the variability in differentiation propensity between hiPSC lines^{21,22}. Another important avenue for future research is to investigate how many specialized cell types can be generated by single or combinatorial TF expression.

As demonstrated here, we envisage that the Human TFome will be a powerful asset in conjunction with other approaches for cell and tissue engineering. As with other genome-scale methods, interpreting the results of Human TFome screens requires information from developmental biology, computational systems biology, cell atlases, functional assays or other sources. In this study, to understand the specific markers for the four analyzed cell types; to learn that the top hit from our screen, *ATOH1*, is involved in neuronal differentiation; to identify *ETV2* as a driver of vascular endothelial programming; to select 15 TFs involved in oligodendrocyte development; and to validate 49 of our hits as previously associated with differentiation, we referred to the developmental biology literature. The systematic, empirical nature of the Human TFome approach is well suited to integration with computational

approaches, such as CellNet⁹, to iteratively refine cell programming. We used CellNet here to identify the phenotype of our second most efficient hit, *NKX3-1*.

For organoid engineering, our orthogonal programming strategy complements existing methods such as assembloids^{55–57}, genetic approaches^{51,58} and in vivo approaches⁵⁹. We overcame the slow emergence of oligodendrocytes in cerebral organoids by including *SOX9*-induced hiPSCs at the beginning of organoid production. Current protocols for myelinated organoids rely on external developmental signaling and require 103–210 d for myelin formation^{36,37}. Orthogonal programming reduced the timeline by more than half, to 40 dpi, to achieve accelerated myelination with mature myelin markers and compact myelin formation with the correct cytoarchitecture. Orthogonal programming might also allow for the incorporation of missing cell types from diverse lineages, distribution of cells more homogeneously within the tissue and fine control over cell proportions, which would all facilitate the adoption of more physiological tissue architecture.

The Human TFome is synergistic with mammalian cell atlases^{35,60–63}. Whereas cell atlas projects ‘read’ cell types and states, the Human TFome enables TF screening aimed at ‘writing’ the cellular programs and has the potential to produce cell types and states that are currently inaccessible. The concepts presented here enable cross-pollination of tissue engineering and genomics to discover recipes for each cell type and state throughout development and aging.

Online content

Any methods, additional references, Nature Research reporting summaries, source data, extended data, supplementary information, acknowledgements, peer review information; details of author contributions and competing interests; and statements of data and code availability are available at <https://doi.org/10.1038/s41587-020-0742-6>.

Received: 3 November 2019; Accepted: 19 October 2020;

Published online: 30 November 2020

References

- Davis, R. L., Weintraub, H. & Lassar, A. B. Expression of a single transfected cDNA converts fibroblasts to myoblasts. *Cell* **51**, 987–1000 (1987).
- Takahashi, K. & Yamanaka, S. Induction of pluripotent stem cells from mouse embryonic and adult fibroblast cultures by defined factors. *Cell* **126**, 663–676 (2006).
- Zhang, Y. et al. Rapid single-step induction of functional neurons from human pluripotent stem cells. *Neuron* **78**, 785–798 (2013).
- Parekh, U. et al. Mapping cellular reprogramming via pooled overexpression screens with paired fitness and single-cell RNA-sequencing readout. *Cell Syst.* **7**, 548–555 (2018).
- Tsunemoto, R. et al. Diverse reprogramming codes for neuronal identity. *Nature* **557**, 375–380 (2018).
- Pritsker, M., Ford, N. R., Jenq, H. T. & Lemischka, I. R. Genomewide gain-of-function genetic screen identifies functionally active genes in mouse embryonic stem cells. *Proc. Natl Acad. Sci. USA* **103**, 6946–6951 (2006).
- Theodorou, E. et al. A high throughput embryonic stem cell screen identifies Oct-2 as a bifunctional regulator of neuronal differentiation. *Genes Dev.* **23**, 575–588 (2009).
- Yamamizu, K. et al. Identification of transcription factors for lineage-specific ESC differentiation. *Stem Cell Rep.* **1**, 545–559 (2013).
- Cahan, P. et al. CellNet: network biology applied to stem cell engineering. *Cell* **158**, 903–915 (2014).
- Rackham, O. J. et al. A predictive computational framework for direct reprogramming between human cell types. *Nat. Genet.* **48**, 331–335 (2016).
- D'Alessio, A. C. et al. A systematic approach to identify candidate transcription factors that control cell identity. *Stem Cell Rep.* **5**, 763–775 (2015).
- Lambert, S. A. et al. The human transcription factors. *Cell* **175**, 598–599 (2018).
- Nakatake, Y. et al. Generation and profiling of 2,135 human ESC lines for the systematic analyses of cell states perturbed by inducing single transcription factors. *Cell Rep.* **31**, 107655 (2020).
- Vaquerez, J. M., Kummerfeld, S. K., Teichmann, S. A. & Luscombe, N. M. A census of human transcription factors: function, expression and evolution. *Nat. Rev. Genet.* **10**, 252–263 (2009).

15. Jolma, A. et al. DNA-binding specificities of human transcription factors. *Cell* **152**, 327–339 (2013).
16. Seiler, C. Y. et al. DNASU plasmid and PSI:Biological-Materials repositories: resources to accelerate biological research. *Nucleic Acids Res.* **42**, D1253–D1260 (2014).
17. Yang, X. et al. A public genome-scale lentiviral expression library of human ORFs. *Nat. Methods* **8**, 659–661 (2011).
18. Wiemann, S. et al. The ORFeome Collaboration: a genome-scale human ORF-clone resource. *Nat. Methods* **13**, 191–192 (2016).
19. Adewumi, O. et al. Characterization of human embryonic stem cell lines by the International Stem Cell Initiative. *Nat. Biotechnol.* **25**, 803–816 (2007).
20. Busskamp, V. et al. Rapid neurogenesis through transcriptional activation in human stem cells. *Mol. Syst. Biol.* **10**, 760 (2014).
21. Choi, J. et al. A comparison of genetically matched cell lines reveals the equivalence of human iPSCs and ESCs. *Nat. Biotechnol.* **33**, 1173–1181 (2015).
22. Cahan, P. & Daley, G. Q. Origins and implications of pluripotent stem cell variability and heterogeneity. *Nat. Rev. Mol. Cell Biol.* **14**, 357–368 (2013).
23. Chanda, S. et al. Generation of induced neuronal cells by the single reprogramming factor ASCL1. *Stem Cell Rep.* **3**, 282–296 (2014).
24. Bermingham, N. A. et al. Math1: an essential gene for the generation of inner ear hair cells. *Science* **284**, 1837–1841 (1999).
25. Sagal, J. et al. Proneural transcription factor Atoh1 drives highly efficient differentiation of human pluripotent stem cells into dopaminergic neurons. *Stem Cells Transl. Med.* **3**, 888–898 (2014).
26. Xue, Y. et al. Synthetic mRNAs drive highly efficient iPS cell differentiation to dopaminergic neurons. *Stem Cells Transl. Med.* **8**, 112–123 (2019).
27. Dutta, A. et al. Identification of an NKX3.1-G9a-UTY transcriptional regulatory network that controls prostate differentiation. *Science* **352**, 1576–1580 (2016).
28. Mai, T. et al. NKX3-1 is required for induced pluripotent stem cell reprogramming and can replace OCT4 in mouse and human iPSC induction. *Nat. Cell Biol.* **20**, 900–908 (2018).
29. Radley, A. H. et al. Assessment of engineered cells using CellNet and RNA-seq. *Nat. Protoc.* **12**, 1089–1102 (2017).
30. Liang, C. C., Park, A. Y. & Guan, J. L. In vitro scratch assay: a convenient and inexpensive method for analysis of cell migration in vitro. *Nat. Protoc.* **2**, 329–333 (2007).
31. Bell, E., Ivarsson, B. & Merrill, C. Production of a tissue-like structure by contraction of collagen lattices by human fibroblasts of different proliferative potential in vitro. *Proc. Natl Acad. Sci. USA* **76**, 1274–1278 (1979).
32. Lee, D. et al. ER71 acts downstream of BMP, Notch, and Wnt signaling in blood and vessel progenitor specification. *Cell Stem Cell* **2**, 497–507 (2008).
33. Baralle, F. E. & Giudice, J. Alternative splicing as a regulator of development and tissue identity. *Nat. Rev. Mol. Cell Biol.* **18**, 437–451 (2017).
34. Potter, R. F. & Groom, A. C. Capillary diameter and geometry in cardiac and skeletal muscle studied by means of corrosion casts. *Microvasc. Res.* **25**, 68–84 (1983).
35. Schaum, N. et al. Single-cell transcriptomics of 20 mouse organs creates a *Tabula Muris*. *Nature* **562**, 367–372 (2018).
36. Madhavan, M. et al. Induction of myelinating oligodendrocytes in human cortical spheroids. *Nat. Methods* **15**, 700–706 (2018).
37. Marton, R. M. et al. Differentiation and maturation of oligodendrocytes in human three-dimensional neural cultures. *Nat. Neurosci.* **22**, 484–491 (2019).
38. Garcia-Leon, J. A. et al. SOX10 single transcription factor-based fast and efficient generation of oligodendrocytes from human pluripotent stem cells. *Stem Cell Rep.* **10**, 655–672 (2018).
39. Ehrlich, M. et al. Rapid and efficient generation of oligodendrocytes from human induced pluripotent stem cells using transcription factors. *Proc. Natl Acad. Sci. USA* **114**, E2243–E2252 (2017).
40. Sarkar, A. & Hochedlinger, K. The sox family of transcription factors: versatile regulators of stem and progenitor cell fate. *Cell Stem Cell* **12**, 15–30 (2013).
41. Bi, W., Deng, J. M., Zhang, Z., Behringer, R. R. & de Crombrughe, B. Sox9 is required for cartilage formation. *Nat. Genet.* **22**, 85–89 (1999).
42. Canals, I. et al. Rapid and efficient induction of functional astrocytes from human pluripotent stem cells. *Nat. Methods* **15**, 693–696 (2018).
43. Khoshakhlagh, P., Sivakumar, A., Pace, L. A., Sazer, D. W. & Moore, M. J. Methods for fabrication and evaluation of a 3D microengineered model of myelinated peripheral nerve. *J. Neural Eng.* **15**, 064001 (2018).
44. Khoshakhlagh, P. & Moore, M. J. Photoreactive interpenetrating network of hyaluronic acid and Puramatrix as a selectively tunable scaffold for neurite growth. *Acta Biomater.* **16**, 23–34 (2015).
45. Mohammadi, S. et al. Whole-brain in-vivo measurements of the axonal G-ratio in a group of 37 healthy volunteers. *Front. Neurosci.* **9**, 441 (2015).
46. Windrem, M. S. et al. Fetal and adult human oligodendrocyte progenitor cell isolates myelinate the congenitally dysmyelinated brain. *Nat. Med.* **10**, 93–97 (2004).
47. Lancaster, M. A. et al. Cerebral organoids model human brain development and microcephaly. *Nature* **501**, 373–379 (2013).
48. Togo, S. et al. Differentiation of embryonic stem cells into fibroblast-like cells in three-dimensional type I collagen gel cultures. *In Vitro Cell. Dev. Biol. Anim.* **47**, 114–124 (2011).
49. Elcheva, I. et al. Direct induction of haematoendothelial programs in human pluripotent stem cells by transcriptional regulators. *Nat. Commun.* **5**, 4372 (2014).
50. Morita, R. et al. ETS transcription factor ETV2 directly converts human fibroblasts into functional endothelial cells. *Proc. Natl Acad. Sci. USA* **112**, 160–165 (2015).
51. Cakir, B. et al. Engineering of human brain organoids with a functional vascular-like system. *Nat. Methods* **16**, 1169–1175 (2019).
52. Woltjen, K. et al. piggyBac transposition reprograms fibroblasts to induced pluripotent stem cells. *Nature* **458**, 766–770 (2009).
53. Ronaldson-Bouchard, K. & Vunjak-Novakovic, G. Organs-on-a-Chip: a fast track for engineered human tissues in drug development. *Cell Stem Cell* **22**, 310–324 (2018).
54. Guye, P. et al. Genetically engineering self-organization of human pluripotent stem cells into a liver bud-like tissue using Gata6. *Nat. Commun.* **7**, 10243 (2016).
55. Bagley, J. A., Reumann, D., Bian, S., Levi-Strauss, J. & Knoblich, J. A. Fused cerebral organoids model interactions between brain regions. *Nat. Methods* **14**, 743–751 (2017).
56. Birey, F. et al. Assembly of functionally integrated human forebrain spheroids. *Nature* **545**, 54–59 (2017).
57. Xiang, Y. et al. Fusion of regionally specified hPSC-derived organoids models human brain development and interneuron migration. *Cell Stem Cell* **21**, 383–398 (2017).
58. Cederquist, G. Y. et al. Specification of positional identity in forebrain organoids. *Nat. Biotechnol.* **37**, 436–444 (2019).
59. Mansour, A. A. et al. An in vivo model of functional and vascularized human brain organoids. *Nat. Biotechnol.* **36**, 432–441 (2018).
60. Rozenblatt-Rosen, O., Stubbington, M. J. T., Regev, A. & Teichmann, S. A. The Human Cell Atlas: from vision to reality. *Nature* **550**, 451–453 (2017).
61. Han, X. et al. Construction of a human cell landscape at single-cell level. *Nature* **581**, 303–309 (2020).
62. Cusanovich, D. A. et al. A single-cell atlas of in vivo mammalian chromatin accessibility. *Cell* **174**, 1309–1324 (2018).
63. Moss, J. et al. Comprehensive human cell-type methylation atlas reveals origins of circulating cell-free DNA in health and disease. *Nat. Commun.* **9**, 5068 (2018).

Publisher's note Springer Nature remains neutral with regard to jurisdictional claims in published maps and institutional affiliations.

© The Author(s), under exclusive licence to Springer Nature America, Inc. 2020

Methods

Annotation of human TFs. A starting set of 1,591 TFs¹⁴ was used, based on their evidence codes “a” and “b” (confirmed experimental evidence), “c” (prediction only) and “other” (probable TFs with undefined DNA-binding domains). Additional TFs curated by the Human Genome Organization’s HUGO Gene Nomenclature Committee (HGNC)⁶⁴ were added: zinc fingers (including those containing C2H2 domains), homeodomains (including LIM, POU, TALE, HOXL, NKL and PRD sub-families) and basic helix-loop-helix and forkhead TFs. Pseudogenes, as annotated by HGNC or Ensembl, were removed. All genes were converted to approved gene names using the HGNC multi-symbol checker. The final set of TFs included in the Human TFome contained 1,564 genes (Supplementary Table 1).

Construction of the Human TFome expression library. Gateway-compatible ORFs for the target set of 1,564 genes were requested from the Vidal lab ORFome collection¹⁸, the Taipale lab¹⁵, DNASU¹⁶ and transOMIC.com. For the missing ORFs, Uniprot protein sequences of 273 genes were reverse-translated and codon-optimized for synthesis by Gen9. Where multiple isoforms exist, the one designated as “canonical” by Uniprot was selected. If the isoform was longer than 4 kb, the longest isoform below 4 kb was chosen owing to synthesis constraints. Synthesized genes were cloned into pDONR221 using BP Clonase II (Invitrogen, 11789020). All pDONR plasmids are available on Addgene, DNASU or transOMIC. TF Sources are summarized in Supplementary Fig. 1a. To determine the tissue expression of synthesized TFs, GTEx²⁰ version 6 median tissue FPKMs were downloaded. For each TF, its median expression across tissues was computed. TFs that were synthesized were compared to TFs that were cloned from cDNAs.

Pooled library cloning into lentiviral expression vector. All pDONR-TFs were pooled and cloned into pLIX_403, the doxycycline-inducible lentiviral vector (a gift from David Root; Addgene plasmid no. 41395), using LR Clonase II (Invitrogen, 11789100), transformed into Stbl3 chemically competent cells (Invitrogen, C737303) and spread on LB agar plates containing 100 µg µl⁻¹ of carbenicillin (Teknova, E0096). Colonies were counted to ensure library coverage of >200×, scraped and resuspended in PBS, and plasmids were extracted using the endotoxin-free Midi Prep Plus Kit (Qiagen, 12943). DNA was quantified using the Qubit dsDNA broad range kit (Invitrogen, Q32853). To determine coverage, pDONR-TF and pLIX_403-TF pools were prepared for next-generation sequencing using the NEBNext Ultra DNA Library Prep Kit for Illumina (New England Biolabs, E7370L). Libraries were quantified using the KAPA Real-Time Library Amplification Kit (Roche, KK2702) and loaded onto an Illumina MiSeq v3 150-cycle kit (MS-102-3001). About 97% of the TFs fit within the pLIX_403 vector cargo limit of approximately 4 kb (Supplementary Fig. 1e). The TF library was subcloned into the lentiviral expression vector with even representation and high coverage (Supplementary Fig. 1f–h).

Data processing and analysis for library cloning. To align reads to the TFome library, reference TF sequences were first indexed using the STAR aligner v2.5.2a7 using the command STAR --runMode genomeGenerate with parameter --genomeSAindexNbases 9 to accommodate a reference ‘genome’ with fewer bases, as recommended in the manual. Reads were aligned to the reference index using the STAR command, counted using bash scripts and plotted in R.

Cell culture. The PGP1 hiPSC line without integrated Yamanaka factors was generated from adult dermal fibroblasts from a 55-year-old male (Coriell, GM23248)⁶⁶, and the CRTD5 hiPSC line⁶⁷ was generated from foreskin fibroblasts (ATCC CRL-2522), both using the CytoTune 2.0 Sendai Reprogramming Kit (Invitrogen, A16517). Cells were adapted to feeder-free culture, verified for pluripotency by flow cytometry and karyotyped. The ATCC DYS0100 hiPSC (ACS-1019 DYS0100) hiPSC was obtained from ATCC. Cell lines were verified by short tandem repeat profiling (Dana-Farber Cancer Institute), regularly verified to be mycoplasma free using the Universal Mycoplasma Detection Kit (ATCC, 30-1012K) and cultured between passages 8 and 40. hiPSCs were cultured in mTeSR1 (STEMCELL Technologies, 05850) without antibiotics on tissue-culture-treated plates coated with Matrigel (Corning, 354277), and media were changed daily. hiPSCs were passaged using TrypLE Express (Life Technologies, 12604013) and seeded with Y-27632 ROCK inhibitor (Millipore, 688001) for 1 d. Cells were frozen using mFreSR (STEMCELL Technologies, 5854) using a CoolCell LX (BioCision, BCS-405) overnight at -80 °C and then in vapor-phase liquid nitrogen for long-term storage. PBAN, a Gateway-compatible, doxycycline-inducible, puromycin-selectable PiggyBac vector was constructed from PB-TRE-dCas9-VPR (Addgene no. 63800) and used to deliver TFs to hiPSCs using a Lonza Nucleofector X-Unit (AAF-1002X), following the manufacturer’s instructions. Electroporated cells were transferred to a six-well Matrigel-coated plate in mTeSR1 with ROCK inhibitor. Cells were selected with 1 µg ml⁻¹ of puromycin (Gibco, A1113803).

Flow cytometry and FACS. For flow cytometry analysis and FACS, cells were dissociated using TrypLE Express, washed and resuspended in FACS buffer (PBS with 10% FBS). For surface antigens, live cells were stained with fluorophore-conjugated antibodies and CellTrace Calcein Blue, AM (Life

Technologies, C34853) at 1 × 10⁷ cells per ml for 30 min on ice in the dark. For intracellular staining, cells were fixed using BD Cytofix fixation buffer (BD Biosciences, 554655) at 1 × 10⁷ cells per ml for 20 min, washed with BD Perm/Wash buffer (BD Biosciences, 554723) and permeabilized in BD Perm/Wash buffer for 10 min and then stained with fluorophore-conjugated antibodies and DAPI in the dark for 30 min. Stained cells were washed twice with FACS buffer, filtered into a strainer-capped tube (Falcon, 352235) and run on a BD LSRFortessa. FACS was performed on a BD FACSAria or Beckman Coulter MoFlo Astrios. Spectral overlap was compensated using single fluorophore-conjugated AbC Total Antibody Compensation Beads (Life Technologies, A10497) with single fluorophore-conjugated antibodies. All antibodies are listed in the table below. Flow cytometry data were analyzed using FlowJo 10.2.

Antibodies used in this study.

Name	Vendor	Catalog number
PE anti-TRA-1-60	BD Biosciences	560193
PE anti-NANOG	BD Biosciences	560483
PerCP-Cy5.5 anti-Oct3/4	BD Biosciences	560794
Alexa 647 anti-SOX2	BD Biosciences	560294
BV421 anti-NCAM	BioLegend	318328
APC anti-NCAM	BD Biosciences	555518
FITC anti-VE-cadherin	BD Biosciences	560411
Alexa 647 anti-VE-cadherin	BD Biosciences	561567
Alexa 488 anti-vimentin	BD Biosciences	562338
APC anti-O4	R&D Systems	FAB1326A
Anti-NG2	BD Biosciences	562415
Anti-MBP	Millipore	MAB386
Anti-MOG	Abcam	ab115597
Anti-vimentin	R&D Systems	AF2105
Anti-HSP47	R&D Systems	MAB91661-100
Anti-ALCAM	R&D Systems	AF1172-SP
Anti-TUBB3	Millipore	AB9354
Anti-NF200	Sigma-Aldrich	N4142
Anti-NeuN	Synaptic Systems	266 004
Anti-V5	Thermo Fisher Scientific	R960-25
Anti-VE-cadherin	Cell Signaling Technologies	2500 P
Human-specific anti-CD31	Dako	M0823
Anti-α-smooth muscle actin	Abcam	ab5694
Anti-MAP2	Abcam	ab92434
Alexa 488 anti-mouse IgG	Invitrogen	A21202
Alexa 647 anti-mouse IgG	Invitrogen	A31571
Alexa 568 anti-goat IgG	Invitrogen	A11057
Alexa 647 anti-goat IgG	Invitrogen	A21447
Alexa 488 anti-rabbit IgG	Invitrogen	A21208
Alexa 555 anti-rabbit IgG	Invitrogen	A31572
Cy3 anti-chicken IgG	Jackson ImmunoResearch	703-165-155
Biotinylated anti-rat IgG	Vector Laboratories	BA-9401

Lentiviral production and transduction. Lentiviral particles were produced as previously described⁶⁸ as one pool containing the complete Human TFome library. Particles were produced by transfecting polyethylenimine (PolyScience, 24765), pMD2G (Addgene, plasmid no. 12259), psPAX2 (Addgene, plasmid no. 12260) and pLIX_403-TFs into 293T cells. Media were exchanged after 24 h, and supernatants were harvested at 48 h and 72 h after transfection. The supernatants were filtered (0.45-µm PES filter, Corning 431220) and combined. Viral particles were then precipitated at 4 °C overnight using PEG solution (BioCat, K904-50-BV). The lentiviral particles were resuspended with PBS in 1/100 of the supernatant volume (100× concentrated). Alternatively, lentiviral particles were concentrated by ultracentrifugation as previously described⁶⁸. The particles were transferred as 50-µl aliquots into 1.5-ml screw-cap tubes, snap-frozen on dry ice and stored at -80 °C. Titrations were performed by quantitative polymerase chain reaction (PCR) as previously described⁶⁸. The titers ranged between 1 × 10⁶ and 6 × 10⁷ IFU ml⁻¹. To transduce the entire library to achieve single-copy integrations, we used a large hiPSC population so that, on average, every TF was theoretically represented by more than 100 cells. Next, 750,000 PGP1, ATCC-DYS0100 and CRTD5 hiPSCs were each transduced with 75,000 lentiviral particles (MOI = 0.1) in mTeSR1

media (two six-well plates per pool). The low MOI ensures that most cells are not transduced (and are, thus, selected against by puromycin), and the cells that are transduced are most likely to receive only a single TF. Culture medium was exchanged daily. Forty-eight hours after transduction, $3\ \mu\text{g ml}^{-1}$ of puromycin was added to the media to eliminate non-transduced PGP1 cells. Cells were maintained and propagated as mentioned before.

TFome screen using FACS. Each independently transduced hiPSC population was expanded into three 10-cm dishes, representing three replicates (Supplementary Fig. 2a). Each dish was seeded with 2 million cells in mTeSR1 with ROCK inhibitor, $0.5\ \mu\text{g ml}^{-1}$ of doxycycline and $1\ \mu\text{g ml}^{-1}$ of puromycin. The next day and daily thereafter until 4 dpi, the media were replenished with mTeSR1 containing doxycycline. As hiPSCs became confluent at 4 dpi, this day was chosen for dissociation and staining. Cells were not passaged for longer culture because of the faster proliferation rate of hiPSCs, which might out-compete differentiated cells. Cells were then dissociated using TrypLE Express and counted using an automated cell counter (Thermo Fisher Scientific, Countess II, AMQAX1000). Typically, 10 million live cells were harvested per 10-cm dish, stained for PE anti-TRA-1-60 and Calcein AM (Life Technologies, C1430) in mTeSR1 media at 10^7 cells per ml for 30 min in the dark, washed and then filtered for debris using a single-cell strainer (Falcon, 352253). Cells were sorted on a BD FACSARIA or a Beckman Coulter MoFlo Astrios. After gating Calcein AM-positive cells, cells in the bottom 10% and the middle 50% of TRA-1-60 expression were designated as TRA-1-60^{low} (differentiation gate) and TRA-1-60^{high} (stem cell gate), respectively. Approximately 0.8 million TRA-1-60^{low} and 4 million TRA-1-60^{high} cells were collected for each replicate in the whole-library screen. Cells were subsequently spun down, and the cell pellet was frozen at -20°C .

Genomic extraction, PCR and library preparation for sequencing. Genomic DNA was extracted from sorted cells using the DNeasy Blood & Tissue Kit (Qiagen, 69506) on a QIAcube (Qiagen). More than $5\ \mu\text{g}$ of genomic DNA was used for PCR and subsequently purified using the QIAquick PCR Purification Kit (Qiagen, 28106) on a QIAcube. Purified DNA was quantified using the Qubit dsDNA broad range quantification kit (Thermo Fisher Scientific, Q32853). One microgram of DNA was sheared to an average of 200 bp on a Covaris sonicator E220 and used for library preparation using NEBNext Ultra DNA Library Prep (New England Biolabs, E7370). Samples were sequenced on an Illumina NextSeq 500 on high-output mode (Supplementary Table 2) with high coverage (Supplementary Fig. 1j).

Analysis of sequencing data from TFome screening. Sequencing reads of amplified TFs were aligned to reference sequences using STAR aligner v2.5.2a⁶⁹. The ratio of cells in TRA-1-60 high versus low gates was used as an indicator of loss of pluripotency above basal spontaneous differentiation for each TF, as the TRA-1-60 high fraction served as an internal control. A $\log_2(\text{TRA-1-60}^{\text{low}}/\text{TRA-1-60}^{\text{high}})$ score was computed using DESeq2 (ref. ⁷⁰). A statistical threshold for defining TFs as hits was determined based on maximizing enrichment compared to random sampling as follows. For each cell line, TFs were ordered by their $\log_2(\text{TRA-1-60}^{\text{low}}/\text{TRA-1-60}^{\text{high}})$ score. Then, an enrichment score was computed for each candidate threshold. The enrichment score is computed by the number of TFs above that threshold in at least two cell lines minus the number of TFs above that threshold in a randomized dataset ($n = 10,000$ random samples). The enrichment scores for a set of candidate thresholds are plotted in Supplementary Fig. 2d. A threshold of 25% had the highest enrichment score.

Literature search to determine novelty of hits. To determine if a TF hit was novel for its ability to induce differentiation or forward programming upon overexpression, the name of each TF hit and the terms 'differentiation', 'programming' or 'overexpression' were queried in PubMed on April 26, 2020. TFs were considered 'known' if at least one paper reported that the overexpression of the TF alone, or in combination with other factors, promoted the differentiation of one cell type into another; otherwise, the TF was considered novel. TFs having knockout studies alone without overexpression evidence were considered novel.

Immunofluorescence microscopy. Cells were immunostained as previously described²⁰. Cells were grown on Matrigel-coated 12-mm coverslips (Warner Instruments, CS-12R15), fixed with 4% paraformaldehyde (PFA) (Electron Microscopy Sciences, 15714-S) in PBS for 20 min at room temperature, washed three times with PBS and kept at 4°C submerged in PBS until staining. Fixed samples were incubated with a blocking solution containing 10% normal donkey serum (NDS, Millipore, S30-100ml), 1% BSA and 0.5% Triton X-100 in $1\times$ PBS for 1 h at room temperature or overnight at 4°C . The stain buffer was similar to the block solution, except the concentration of NDS was reduced to 3%. Coverslips were incubated at room temperature for 1 h with the stain buffer containing primary antibodies and then washed with stain buffer twice, incubated with secondary antibodies in stain buffer at room temperature for 1 h and washed once with stain buffer and twice with PBS. Coverslips were mounted on glass slides by incubating with Prolong Diamond Antifade with DAPI (Invitrogen, P36966), incubated overnight at room temperature in the dark and sealed with nail polish

(Electron Microscopy Sciences, 72180). Mounted coverslips were imaged on a Zeiss Observer.Z1 microscope equipped with a LD Plan-Neofluar $\times 40/0.6$ objective, a four-channel LED light source (Colibri) and an EM-CCD digital camera system (Hamamatsu).

Bulk RNA-seq library preparation. Six hundred microliters of TRIzol (Life Technologies, 15596-018) was added directly to cells, which were then incubated for 3 min and used for RNA extraction using Direct-zol RNA MiniPrep, following the manufacturer's recommendations (Zymo Research, R2050). RNA was quantified using the Qubit RNA HS Kit (Molecular Probes, Q32852), and RNA integrity was confirmed by the presence of intact 18S and 28S bands on a 1% E-Gel EX (Invitrogen, G402001). One microgram of RNA was used for Poly(A) isolation using the NEBNext Poly(A) mRNA Magnetic Isolation Module (New England Biolabs, E7490L) and the NEBNext Ultra Directional RNA Library Prep Kit for Illumina (New England Biolabs, E7420L). Library size was visualized on a 1% E-Gel EX and quantified using the KAPA Library Quantification Kit, as described before. Samples were sequenced on an Illumina NextSeq500 on high-output mode.

Analysis of bulk RNA-seq data. A STAR human transcriptome reference index was generated using Gencode GRCh38.primary (ftp://ftp.sanger.ac.uk/pub/gencode/Gencode_human/release_25/GRCh38.primary_assembly.genome.fa.gz) as the genome sequence and Gencode v25 transcript annotations (ftp://ftp.sanger.ac.uk/pub/gencode/Gencode_human/release_25/gencode.v25.annotation.gtf.gz). RNA-seq reads were aligned on four 12-Gb cores using the command: STAR -quantMode GeneCounts. Gene counts per sample were merged into a master table and analyzed in R version 3.2.2. Differential expression analysis was performed using DESeq2 (ref. ⁷⁰). The \log_2 fold changes and standard errors were estimated using DESeq2. The default Wald's test was used for statistical testing, independent filtering and P value adjustments. Heat maps were generated in R using the gplots and RColorBrewer packages. Default settings were used for scaling, coloring and clustering. CellNet[®] was used on FASTQ files to classify cell types using default settings. FASTQ files are available in the National Center for Biotechnology Information's Gene Expression Omnibus (see the 'Data availability' section).

Comparison of RNA data to reference datasets. Bulk RNA-seq raw data for *ATOH1*, *NKX3-1*, *ETV2* and *SOX9*-induced cells and external reference datasets were processed consistently using the identical pipeline for gene expression quantification. Gene expression profiles of *ATOH1*-induced neurons were compared to human brain samples from the ENCODE Project (ENCSR239GFM for hippocampus and ENCSR274JRR for brain). *SOX9*-induced oligodendrocytes were compared to newly formed oligodendrocytes, myelinating oligodendrocytes and oligodendrocyte precursor cells collected from mouse brain⁷¹ (GSE52564). *NKX3-1*-induced fibroblasts were compared to fibroblasts²¹ (GSE73211). *ETV2*-induced endothelial cells were compared to human umbilical cord endothelial cells (HUVECs)⁷² (GSE93511). Gene counts were calculated by RSEM (1.3.3)⁷³ with the --star option to use reads aligned with STAR (2.7.3a) to the GRCh38 reference genome and Ensembl annotation 94. Secondary analyses were performed in the statistical R environment (v3.6.1). TPM values from the RSEM output were used for gene filtering and PCA. Genes with more than 10 counts per million in at least three samples were retained. For the comparison between *SOX9*-induced cells and mouse OPCs, only homologous genes between the two species annotated in the Mouse Genome Database⁷⁴ (http://www.informatics.jax.org/downloads/reports/HOM_MouseHumanSequence.rpt) were retained. A DESeq2 (ref. ⁷⁰) object was created providing the cell line information in the design formula. PCA was then performed on vst transformed⁷⁵ and SVA batch corrected⁷⁶ TPM values using the prcomp function. Removal of hPSCs before PCA did not affect the separation between differentiated and primary cells.

Electrophysiology. Assessment of neuronal function was performed as previously described²⁰ with minor modifications. Rat astrocytes (Gibco, N7745100) were seeded onto Matrigel-coated coverslips and cultured in DMEM with GlutaMAX, 10% FBS and N2 supplement (Gibco, 17502048). One day before seeding induced neurons, astrocytes were cultured in Neurobasal media with GlutaMAX and B27 supplement (Gibco, 17504044). *ATOH1* hiPSCs were labeled by lentiviral transduction of constitutively expressed green fluorescent protein (GFP) (FUGW, Addgene no. 14883). Next, 500,000 GFP-labeled *ATOH1* hiPSCs were seeded in a six-well tissue culture plate and induced with doxycycline for 3 d on Matrigel-coated coverslips and then dissociated using TrypLE Express. Cells were counted, and 1 million induced neurons were plated in pre-conditioned media on astrocytes. Media were changed twice weekly. Electrophysiological recordings were carried out at $20\text{--}25^\circ\text{C}$ on an upright Olympus BX51WI microscope. Cells were bathed in artificial cerebrospinal fluid containing (in mM) 119 NaCl, 2.5 KCl, 4 CaCl₂, 4 MgSO₄, 1 NaH₂PO₄, 26.2 NaHCO₃, and 11 glucose and saturated with 95% O₂/5% CO₂. Intracellular recordings were obtained using 3- to 5-M Ω glass micropipettes filled with an internal solution containing (in mM) 136 KMeSO₃, 17.8 HEPES, 0.6 MgCl₂, 1 EGTA, 4 Mg-ATP and 0.3 Na-GTP. Traces were collected using a MultiClamp 700B amplifier (Molecular Devices), filtered with a 2-kHz Bessel filter, digitized at 10 kHz using a Digidata 1440A digitizer (Molecular Devices), stored using Clampex 10 (Molecular Devices) and analyzed offline using customized procedures in IGOR Pro (WaveMetrics). Cells were assessed for the

were carried out in five mice, and explants were harvested after 1 week. Human mesenchymal stromal cells (hMSCs) were isolated from the white adipose tissue and cultured on uncoated plates using MSCGM (Lonza, cat. no. PT-3001) supplemented with 10% Gencode FBS (Genesee, cat. no. 25-514) and 1X penicillin–streptomycin–glutamine (Thermo Fisher Scientific, cat. no. 10378106). All experiments were carried out using passage 6–10 hMSCs.

Implanted grafts were fixed overnight in 10% buffered formalin, embedded in paraffin and sectioned at a thickness of 7 µm. Microvessel density (vessels per mm²) was defined as the average number of erythrocyte-filled vessels in hematoxylin and eosin (H&E)-stained sections collected from the middle of the implants, as previously described^{82,83}. For immunostainings, sections were deparaffinized, and antigen retrieval was carried out for 30 min with boiling citric buffer (10 mM sodium citrate and 0.05% Tween 20, pH 6.0). Sections were then blocked for 30 min in 5% horse serum and incubated with primary antibodies for 30 min at room temperature. Fluorescent staining was performed using fluorophore-conjugated secondary antibodies, followed by DAPI counterstaining for 30 min at room temperature. Human-specific anti-CD31 (Dako, M0823) was used to stain human blood vessels. Perivascular cells were stained by anti-α-SMA antibody (Abcam, ab5694). Images were acquired using an Axio Observer Z1 inverted microscope (Carl Zeiss) and AxioVision Rel. 4.8 software. Fluorescent images were acquired using an ApoTome.2 Optical sectioning system (Carl Zeiss) using a ×20 objective lens.

In vitro myelination assay. SOX9-induced oligodendrocytes were co-cultured with iNGN hiPSC-derived neurons²⁰ to assess myelin formation. To facilitate the preparation of cross-sections of myelinated axons, these cells were co-cultured within a microchannel mold that promotes the alignment of axons along the channel in one direction. The microchannel mold was constructed by adding a 10% (wt/vol) PEG-diacrylate (Mn 1000; Polysciences) and 0.5% (wt/vol) Irgacure 2959 in PBS solution to a collagen-coated transwell^{43,84,85}. A negative mask was used to create the microchannel, followed by irradiation of the light-sensitive media with 181 mW cm⁻² ultraviolet light for 30 s. SOX9 and iNGN hiPSCs were then seeded into the microchannel, and TFs were induced by doxycycline. The co-culture was maintained in mTeSR1 for the first 4 d, and then the media were replaced to preserve long-term oligo-neuronal culture with the following components: DMEM-F12 with 1:200 N2 supplement, 1:100 B27 supplement lacking vitamin A, 1% penicillin–streptomycin–glutamine, 60 ng ml⁻¹ of T3, 10 ng ml⁻¹ of NT3, 10 ng ml⁻¹ of IGF-I, 200 µM AA, 1:1,000 Trace Elements B, 2 ng ml⁻¹ of BDNF and 2 ng ml⁻¹ of GDNF³⁹. After 4 weeks of co-culture, the constructs were fixed, embedded in resin, sectioned, stained and imaged using TEM as described above for the angiogenesis assay.

In vivo engraftment and myelination assay. Homozygous Shiverer mice⁴⁶ were purchased from Jackson Laboratories (stock no. 001428), housed under appropriate conditions and crossed with heterozygous mice adhering to Harvard Medical School guidelines. All animal protocols were approved by the Institutional Animal Care and Use Committee. Four-day doxycycline-induced SOX9 cells were live stained⁴⁶ using 1:10 O4 antibody and sorted for O4-positive cells using a Sony SH800s cell sorter. Neonatal mice (postnatal days 1–2) were cryo-anesthetized, and 50,000 O4-positive cells resuspended in 2 µl of PBS were injected intracranially by freehand injection⁴⁶. Control animals received PBS injections. Pups in both control and experimental groups were confirmed to be homozygous Shiverer both by their phenotype and through genotyping and were euthanized for further analysis after 10 weeks using perfusion with 4% PFA. Tissue sections were obtained and embedded for antibody staining. Briefly, the brain sections were de-paraffinized, and an antigen retrieval process was done in a sodium citrate buffer at 95 °C for 30 min. The slides were then blocked with 10% normal goat serum in 1% BSA in PBS for 30 min at room temperature, followed by staining using anti-MBP antibodies in 1% BSA in PBS overnight at 4 °C. The next day, the slides were washed with PBS and incubated with 1:250 biotinylated goat anti-rat secondary antibodies. After multiple washing steps, the slides were counterstained by hematoxylin, dehydrated and mounted. To perform electron microscopy on the brain tissue, the injection site was used as a landmark to prepare the tissue for sectioning. The rest of the process was done similarly to what has been described earlier for electron microscopy.

Parallel cell programming in two-dimensional culture. For immunofluorescence microscopy, *ATOHI1*, *ETV2* and *NKX3-1* hiPSCs were mixed and seeded in all combinations at equal ratios in mTeSR1 and Y-27632 ROCK inhibitor with or without 0.5 µg ml⁻¹ of doxycycline on Matrigel-coated 10-mm circular coverslips in 12-well plates. In total, 60,000 cells were seeded in wells for non-induced controls and 180,000 in wells for doxycycline induction. mTeSR1 with or without doxycycline was replenished each day. After 4 d, the medium was removed, and cells were washed with PBS (without magnesium or calcium) at room temperature and fixed in 4% PFA (Electron Microscopy Sciences, 15714-S) in PBS for 15 min at room temperature. Coverslips were blocked with 200 µl of 10% NDS (Millipore, S30–100 ml) in PBS for 20 min and incubated for 90 min at room temperature with the following primary antibodies diluted in 3% NDS in PBS: 1:400 rabbit anti-VE-cadherin, 1:500 chicken anti-MAP2 and 1:400 goat anti-ALCAM. After three 10-min washes with 200 µl of PBS, coverslips were incubated for 45 min

at room temperature with fluorophore-conjugated secondary antibodies (1:500 dilution) and 1 mg ml⁻¹ of DAPI (Roche, 10236276001) in 3% NDS: donkey anti-chicken Cy3, donkey anti-rabbit Alexa Fluor 488 and donkey anti-goat Alexa 647. Coverslips were then mounted on microscopy slides using AquaMount (VWR, 41799-008) and stored overnight in the dark at room temperature. Thereafter, slides were imaged with an Axio Observer.Z1 microscope with motorized stage (Carl Zeiss Microscopy) using ×20 and ×40 air objectives. Images were stored in the manufacturer's format (.czi) and subsequently exported to the *.jpeg format using ZEN blue software (Carl Zeiss Microscopy).

For flow cytometry and single-cell sorting, *ATOHI1*, *ETV2* isoform 2 and *NKX3-1* hiPSCs were mixed and seeded in all combinations in mTeSR1 and Y-27632 ROCK inhibitor with or without 0.5 µg ml⁻¹ of doxycycline on Matrigel-coated 12-well plates. In total, 30,000 cells were seeded in wells for non-induced controls and 90,000 in wells for doxycycline induction. mTeSR1 with or without doxycycline was replenished daily. After 4 d, cells were dissociated with TrypLE Express, re-suspended with 1 ml of PBS per well, transferred to strainer-capped tubes for flow cytometry and spun down for 4 min at 1,400 r.p.m. Next, the supernatant was aspirated, and cells were immunofluorescently labeled with fluorophore-conjugated antibodies against NCAM (1:20), vimentin (1:20) and VE-cadherin (1:20) diluted in 100 µl of 0.2 µm-filtered FACS buffer (1% BSA (albumin fraction V; Roth, 8076.2) and 2 mM EDTA, in sterile PBS pH 7.4) for 1 h at 4 °C in the dark. Cells were spun down for 4 min at 1,400 r.p.m., washed with FACS buffer once, spun down again and re-suspended in 250 µl of FACS buffer. Tubes were kept on ice until analysis within the next hour on a BD FACSaria II. Additionally, 95 single cells were sorted in a 96-well plate with a BD FACSaria III (100-µm nozzle) and sent for single-cell sequencing at the CMCB Deep Sequencing Facility.

Parallel cell programming in embryoid bodies. Twenty-four-well AggreWell plates (STEMCELL Technologies, 34450) were prepared following the manufacturer's protocol. *ATOHI1*, *ETV2* isoform 2 and *NKX3-1* hiPSCs were seeded in equal ratios in AggreWell EB Formation Medium (STEMCELL Technologies, 05893) with Y-27632 ROCK inhibitor (Millipore, 688001). A total of 6 × 10⁵ cells were used. Fifty percent AggreWell EB Formation Medium was changed daily. After 4 d, the EBs were harvested and transferred into ultra-low attachment wells (Sigma-Aldrich, CLS3471-24EA) using AggreWell EB Formation Medium supplemented with 3 µg ml⁻¹ of puromycin (Life Technologies, A11138-03). TF expression was induced with doxycycline 7 d after seeding.

For flow cytometry analysis, EBs were dissociated using TrypLE Express, washed and resuspended in FACS buffer (PBS with 10% FBS). For surface antigens, live cells were stained with fluorophore-conjugated antibodies at 1 × 10⁷ cells per ml for 30 min on ice in the dark. Stained cells were washed twice with FACS buffer, filtered into a strainer-capped tube (Falcon, 352235) and analyzed on a BD LSRII. Flow cytometry data were analyzed using FlowJo 10.2.

For immunofluorescence microscopy, EBs were fixed with 4% PFA (Electron Microscopy Sciences, 15714-S) in PBS for 30 min at room temperature and then washed three times with PBS and kept at 4 °C in PBS. Next, fixed samples were incubated with blocking solution (10% NDS, 1% BSA and 0.5% Triton X-100 in PBS) for 1 h at room temperature. For staining, a buffer similar to the blocking buffer was used but with reduced NDS (3%). Samples were incubated with primary antibodies at room temperature for 1 h, subsequently washed with staining buffer twice, incubated with secondary antibodies and 1 mg ml⁻¹ of DAPI (Roche, 10236276001) at room temperature for 1 h, washed once with staining buffer and then washed twice with PBS. EBs were finally mounted in 1% agarose on MatTek dishes and immersed in PBS. Stained EBs were imaged on a Zeiss LSM780 upright microscope equipped with a Zeiss Achroplan ×40/0.8 W water dipping (immersion) objective. To maximize signal-to-noise ratios, detector gains were kept between 600 and 900, and laser powers were kept between 1% and 12%. z-stacks were generated and stored in the manufacturer's format (.czi). Maximum intensity projections were exported in ZEN blue software.

Orthogonal cell programming in cerebral organoids. Cerebral organoids were generated as previously described⁴⁷ with minor modifications. To orthogonally program induced oligodendrocytes within cerebral organoids, inducible SOX9 hiPSCs and unmodified hiPSCs were dissociated with TrypLE Express (Life Technologies, 12604013), counted using an automated cell counter (Countess II, AMQAX1000, Thermo Fisher Scientific) and mixed at a ratio of 1:1 in AggreWell medium (STEMCELL Technologies, 05893). Next, the single-cell suspension was transferred to AggreWell400 plates (STEMCELL Technologies, 27945) for embryoid body formation. Then, 600,000 cells were seeded into an AggreWell plate containing AggreWell medium with 10 µM Y-27632 ROCK inhibitor (Millipore, 688001). The plate was spun down at 100g for 3 min and placed in a tissue culture incubator overnight. The next day (day 1 of the protocol), embryoid body formation was verified by bright-field microscopy, and the media were changed to neural induction media (DMEM/F12, HEPES and GlutaMAX (Invitrogen, 11330-032) with N2 supplement (Gibco, A13707-01) and non-essential amino acids (Gibco, 11140-050)). Half of the media were changed daily with neural induction media from days 1–3. On day 4, embryoid bodies were harvested by pipetting gently with a wide-bore tip to dislodge them from the AggreWells and individually embedded in droplets of undiluted Matrigel (Corning, 354277). To

induce TF expression for orthogonal programming, 0.5 µg ml⁻¹ of doxycycline was added daily into the media starting on day 4. On day 8, media were changed to neural differentiation media consisting of 1:1 DMEM/F12 containing HEPES and GlutaMAX (Invitrogen, 11330-032) and Neurobasal medium (Invitrogen, 12348-017) with non-essential amino acids (Gibco, 11140-050), N2 supplement (Gibco, A13707-01) and B27 supplement without vitamin A (Gibco, 12587-010). Media were replaced every other day. Organoids were harvested and sliced onto charged glass slides and stored at -20°C until use. For staining, samples were brought to room temperature and outlined with a wax pen. They were washed three times with MAXwash Washing Medium (ActiveMotif, 15254) to remove any remaining OCT and then blocked using MAXblock Blocking Medium (ActiveMotif, 15252) for 1 h and then washed with MAXwash Washing Medium. Primary antibodies in binding buffer (ActiveMotif, 15251) were added and allowed to stain overnight. Samples were washed three times with wash buffer and then stained for 5 h with secondary antibodies in binding buffer. Samples were washed with wash buffer, stained with DAPI and then mounted for imaging using VECTASHIELD mounting media.

Statistics. All statistics, including statistical tests, sample sizes and types of replicates, are described in the figure legends. Exact *P* values are listed in Supplementary Table 7. *P* values less than 0.05 were considered significant.

Reporting Summary. Further information on research design is available in the Nature Research Reporting Summary linked to this article.

Data availability.

Next-generation sequencing data that support the findings of the study are available in the Gene Expression Omnibus using accession code [GSE159786](https://www.ncbi.nlm.nih.gov/geo/query/acc.cgi?acc=GSE159786).

Code availability

The code that supports the findings of this study is available from the corresponding authors upon reasonable request.

References

64. Gray, K. A., Yates, B., Seal, R. L., Wright, M. W. & Bruford, E. A. Genenames.org: the HGNC resources in 2015. *Nucleic Acids Res.* **43**, D1079–D1085 (2015).
65. Mele, M. et al. Human genomics. The human transcriptome across tissues and individuals. *Science* **348**, 660–665 (2015).
66. Church, G. M. The personal genome project. *Mol. Syst. Biol.* **1**, 2005.0030 (2005).
67. Kutsche, L. K. et al. Combined experimental and system-level analyses reveal the complex regulatory network of miR-124 during human neurogenesis. *Cell Syst.* **7**, 438–452 (2018).
68. Salmon, P. & Trono, D. Production and titration of lentiviral vectors. in *Current Protocols in Human Genetics* Ch. 12, Unit 12.10 (Wiley, 2007).
69. Dobin, A. et al. STAR: ultrafast universal RNA-seq aligner. *Bioinformatics* **29**, 15–21 (2013).
70. Love, M. I., Huber, W. & Anders, S. Moderated estimation of fold change and dispersion for RNA-seq data with DESeq2. *Genome Biol.* **15**, 550 (2014).
71. Zhang, Y. et al. An RNA-sequencing transcriptome and splicing database of glia, neurons, and vascular cells of the cerebral cortex. *J. Neurosci.* **34**, 11929–11947 (2014).
72. Zhang, J. et al. A genome-wide analysis of human pluripotent stem cell-derived endothelial cells in 2D or 3D culture. *Stem Cell Rep.* **8**, 907–918 (2017).
73. Li, B. & Dewey, C. N. RSEM: accurate transcript quantification from RNA-Seq data with or without a reference genome. *BMC Bioinf.* **12**, 323 (2011).
74. Bult, C. J., Blake, J. A., Smith, C. L., Kadin, J. A. & Richardson, J. E. Mouse genome database (MGD) 2019. *Nucleic Acids Res.* **47**, D801–D806 (2019).
75. Anders, S. & Huber, W. Differential expression analysis for sequence count data. *Genome Biol.* **11**, R106 (2010).
76. Leek, J. T. svaseq: removing batch effects and other unwanted noise from sequencing data. *Nucleic Acids Res.* **42**, e161 (2014).
77. Schindelin, J. et al. Fiji: an open-source platform for biological-image analysis. *Nat. Methods* **9**, 676–682 (2012).
78. Ngo, P., Ramalingam, P., Phillips, J. A. & Furuta, G. T. Collagen gel contraction assay. *Methods Mol. Biol.* **341**, 103–109 (2006).
79. Picelli, S. et al. Smart-seq2 for sensitive full-length transcriptome profiling in single cells. *Nat. Methods* **10**, 1096–1098 (2013).
80. Wolf, F. A., Angerer, P. & Theis, F. J. SCANPY: large-scale single-cell gene expression data analysis. *Genome Biol.* **19**, 15 (2018).
81. Liao, Y., Smyth, G. K. & Shi, W. featureCounts: an efficient general purpose program for assigning sequence reads to genomic features. *Bioinformatics* **30**, 923–930 (2014).
82. Koike, N. et al. Tissue engineering: creation of long-lasting blood vessels. *Nature* **428**, 138–139 (2004).
83. Melero-Martin, J. M. et al. Engineering robust and functional vascular networks in vivo with human adult and cord blood-derived progenitor cells. *Circ. Res.* **103**, 194–202 (2008).
84. Khoshakhlagh, P. et al. Development and characterization of a bioglass/chitosan composite as an injectable bone substitute. *Carbohydrate Polym.* **157**, 1261–1271 (2017).
85. Khoshakhlagh, P., Bowser, D. A., Brown, J. Q. & Moore, M. J. Comparison of visible and UVA phototoxicity in neural culture systems micropatterned with digital projection photolithography. *J. Biomed. Mater. Res. A* **107**, 134–144 (2019).
86. Douvaras, P. & Fossati, V. Generation and isolation of oligodendrocyte progenitor cells from human pluripotent stem cells. *Nat. Protoc.* **10**, 1143–1154 (2015).

Acknowledgements

We thank J. Aach, M. O. Karl, R. Kalhor, N. Ostrov and H. Lee for critical feedback and the Church and Busskamp laboratories for support. We acknowledge technical support from the Harvard Biopolymers Facility, the Harvard Division of Immunology Flow Cytometry Core Facility, the Beth Israel Deaconess Medical Center Flow Cytometry Core, the Wyss Flow Cytometry and Microscopy Core, M. Ericsson and P. Coughlin at the Harvard Medical School Electron Microscopy Facility, M. T. Gianatasio at the Dana-Farber/Harvard Cancer Center Specialized Histopathology Core and Rodent Histopathology Core (both supported, in part, by National Cancer Institute Cancer Center Support grant NIH 5 P30 CA06516) and Harvard Medical School Orchestra Research Computing. We also thank the TU Dresden Center for Molecular and Cellular Bioengineering Advanced Imaging, Deep Sequencing, Flow Cytometry and Stem Cell Engineering core facilities. We would also like to thank J. Gray's laboratory for electrophysiology support, S. Jeanty and J. Lee (Church lab, Harvard Medical School) for the PGP1 Sendai virus hiPSC line, G. Sheynkman and W. Glindmeyer for helpful discussions, A. Jolma, K. Nitta and K. Said for technical assistance and M. Lemieux and J. McDade for their support in depositing the library to Addgene. A.H.M.N. was supported by a NSERC Postgraduate Fellowship and a Peter and Carolyn Lynch Foundation Fellowship. J.E.R.A. was supported by the DIGS-BB program. S.L.S. is a Shurl and Kay Curci Foundation Fellow of the Life Sciences Research Foundation. The Ellison Foundation and Institute Sponsored Research funds from the DFCI Strategic Initiative supported M.V. and D.E.H. The project was supported by the Volkswagen Foundation (Freigeist - A110720), the European Research Council (ERC-StG-678071 - ProNeurons) and the Deutsche Forschungsgemeinschaft (SPP2127, EXC-2068-390729961 - Cluster of Excellence - Physics of Life at TU Dresden and EXC-2151-390873048 - Cluster of Excellence - ImmunoSensation² at the University of Bonn) to V.B. G.M.C. acknowledges funding from National Human Genome Research Institute grants P50 HG005550 'Center for Casual Variation', RM1 HG008525 'Center for Genomically Engineered Organs', the Simons Foundation for Autism Research Initiative (368485), the Blavatnik Biomedical Accelerator at Harvard University, the FunGCAT program from the Office of the Director of National Intelligence Intelligence Advanced Research Projects Activity, via the Army Research Office, under federal award no. W911NF-17-2-0089 and research funding from R. Merkin and the Merkin Family Foundation.

Author contributions

A.H.M.N., P.K., V.B. and G.M.C. conceived the idea, led the study and designed all experiments. A.H.M.N. and P.K. performed most of the experiments and analyses, with significant technical contributions from J.E.R.A., G.P., K.W., A.S., S.L.S., E.A., K.K., R.E.K., A.V., M.D., K.L., W.S., J.Y.H., A.G., J.T., D.E.H., M.V. and J.M.M.-M. V.B. and G.M.C. oversaw the study. A.H.M.N., P.K. and V.B. wrote the manuscript with input and feedback from all authors.

Competing interests

A.H.M.N., P.K., V.B. and G.M.C. are inventors on patents filed by the Presidents and Fellows of Harvard College. Full disclosure for G.M.C. is available at <http://arep.med.harvard.edu/gmc/tech.html>. A.H.M.N., P.K. and G.M.C. are co-founders of and have equity in GC Therapeutics, Inc. No reagents or funding from GC Therapeutics were used in this study.

Additional information

Supplementary information is available for this paper at <https://doi.org/10.1038/s41587-020-0742-6>.

Correspondence and requests for materials should be addressed to V.B. or G.M.C.

Reprints and permissions information is available at www.nature.com/reprints.

Reporting Summary

Nature Research wishes to improve the reproducibility of the work that we publish. This form provides structure for consistency and transparency in reporting. For further information on Nature Research policies, see our [Editorial Policies](#) and the [Editorial Policy Checklist](#).

Statistics

For all statistical analyses, confirm that the following items are present in the figure legend, table legend, main text, or Methods section.

n/a Confirmed

- ☐ ☒ The exact sample size (n) for each experimental group/condition, given as a discrete number and unit of measurement
- ☒ ☐ A statement on whether measurements were taken from distinct samples or whether the same sample was measured repeatedly
- ☐ ☒ The statistical test(s) used AND whether they are one- or two-sided
Only common tests should be described solely by name; describe more complex techniques in the Methods section.
- ☒ ☐ A description of all covariates tested
- ☐ ☒ A description of any assumptions or corrections, such as tests of normality and adjustment for multiple comparisons
- ☐ ☒ A full description of the statistical parameters including central tendency (e.g. means) or other basic estimates (e.g. regression coefficient) AND variation (e.g. standard deviation) or associated estimates of uncertainty (e.g. confidence intervals)
- ☒ ☐ For null hypothesis testing, the test statistic (e.g. F , t , r) with confidence intervals, effect sizes, degrees of freedom and P value noted
Give P values as exact values whenever suitable.
- ☒ ☐ For Bayesian analysis, information on the choice of priors and Markov chain Monte Carlo settings
- ☒ ☐ For hierarchical and complex designs, identification of the appropriate level for tests and full reporting of outcomes
- ☐ ☒ Estimates of effect sizes (e.g. Cohen's d , Pearson's r), indicating how they were calculated

Our web collection on [statistics for biologists](#) contains articles on many of the points above.

Software and code

Policy information about [availability of computer code](#)

Data collection Illumina RTA 1.18.54, BD FACSDiva, ZEN 2012 (Blue Edition), QuantaSoft, LightCycler 480 Software

Data analysis STAR v2.5.2a, R v3.2.2, DESeq2 v1.8.2, Fiji v1.0, Adobe Illustrator CS6 v16.0.0, FlowJo 10.4, Microsoft Excel, WaveMetrics Igor Pro, Python

For manuscripts utilizing custom algorithms or software that are central to the research but not yet described in published literature, software must be made available to editors and reviewers. We strongly encourage code deposition in a community repository (e.g. GitHub). See the Nature Research [guidelines for submitting code & software](#) for further information.

Data

Policy information about [availability of data](#)

All manuscripts must include a [data availability statement](#). This statement should provide the following information, where applicable:

- Accession codes, unique identifiers, or web links for publicly available datasets
- A list of figures that have associated raw data
- A description of any restrictions on data availability

Next-generation sequencing data will be uploaded to Gene Expression Omnibus (GEO).

Field-specific reporting

Please select the one below that is the best fit for your research. If you are not sure, read the appropriate sections before making your selection.

☒ Life sciences ☐ Behavioural & social sciences ☐ Ecological, evolutionary & environmental sciences

For a reference copy of the document with all sections, see [nature.com/documents/nr-reporting-summary-flat.pdf](https://www.nature.com/documents/nr-reporting-summary-flat.pdf)

Life sciences study design

All studies must disclose on these points even when the disclosure is negative.

Sample size	No statistical methods were used to predetermine the sample size.
Data exclusions	No data was excluded.
Replication	All findings were reproducible.
Randomization	Samples were not randomized.
Blinding	Investigators were not blinded to experiments.

Reporting for specific materials, systems and methods

We require information from authors about some types of materials, experimental systems and methods used in many studies. Here, indicate whether each material, system or method listed is relevant to your study. If you are not sure if a list item applies to your research, read the appropriate section before selecting a response.

Materials & experimental systems

n/a	Involved in the study
<input type="checkbox"/>	<input checked="" type="checkbox"/> Antibodies
<input type="checkbox"/>	<input checked="" type="checkbox"/> Eukaryotic cell lines
<input checked="" type="checkbox"/>	<input type="checkbox"/> Palaeontology and archaeology
<input type="checkbox"/>	<input checked="" type="checkbox"/> Animals and other organisms
<input checked="" type="checkbox"/>	<input type="checkbox"/> Human research participants
<input checked="" type="checkbox"/>	<input type="checkbox"/> Clinical data
<input checked="" type="checkbox"/>	<input type="checkbox"/> Dual use research of concern

Methods

n/a	Involved in the study
<input checked="" type="checkbox"/>	<input type="checkbox"/> ChIP-seq
<input type="checkbox"/>	<input checked="" type="checkbox"/> Flow cytometry
<input checked="" type="checkbox"/>	<input type="checkbox"/> MRI-based neuroimaging

Antibodies

Antibodies used

This list is also included in the supplementary materials.
 PE anti-TRA-1-60 BD Bioscience 560193
 PE anti-human NANOG BD Bioscience 560483
 PerCP-Cy5.5 anti-Oct3/4 BD Bioscience 560794
 Alexa Fluor 647 anti-Sox2 BD Bioscience 560294
 APC Anti-CD56/NCAM BD Bioscience 555518
 FITC Anti-CD144/VE-Cadherin BD Bioscience 560411
 Alexa Fluor 488 anti-Vimentin BD Bioscience 562338
 Anti-Vimentin R&D Systems AF2105
 Anti-HSP47/SERPINE1 R&D Systems MAB91661-100
 Anti-ALCAM/CD166 R&D Systems AF1172-SP
 Anti-Beta-III-Tubulin/TUBB3 Millipore AB9354
 Anti-NF200 Sigma N4142
 Anti-V5 ThermoFisher R960-25
 Anti-VE-Cadherin Cell Signalling Technologies 2500P
 Alexa Fluor488 donkey anti-mouse IgG (H+L) Life Technologies A21202
 Alexa Fluor647 donkey anti-mouse IgG (H+L) Life Technologies A31571
 Alexa Fluor568 donkey anti-goat IgG (H+L) Life Technologies A11057
 Alexa Fluor647 donkey anti-goat IgG (H+L) Life Technologies A21447
 Alexa Fluor488 donkey anti-rabbit IgG (H+L) Life Technologies A21208
 Alexa Fluor555 donkey anti-rabbit IgG (H+L) Life Technologies A31572
 Donkey anti-chicken-Cy3 Jackson Labs Jackson ImmunoResearch 703-165-155

Validation

We used antibodies with validation data from the vendor's website.

Eukaryotic cell lines

Policy information about [cell lines](#)

Cell line source(s)	The non-integrated PGP1 hiPSC line was generated from adult dermal fibroblasts (Coriell, GM23248) and the CRTD5 hiPSC line was generated from foreskin fibroblasts (ATCC CRL-2522) using the CytoTune 2.0 Sendai Reprogramming Kit (Invitrogen, A16517). The ATCC hiPSC (ACS-1019 DYS0100) hiPSC was obtained from ATCC.
Authentication	Cell lines were verified by short tandem repeat (STR) profiling (Dana Farber Cancer Institute).
Mycoplasma contamination	Cells were tested negative for mycoplasma using the Universal Mycoplasma Detection Kit (ATCC, 30-1012K),
Commonly misidentified lines (See ICLAC register)	No commonly misidentified lines were used.

Animals and other organisms

Policy information about [studies involving animals](#); [ARRIVE guidelines](#) recommended for reporting animal research

Laboratory animals	Six-week-old NOD/SCID mice and Shiverer mice were purchased from Jackson Laboratories.
Wild animals	The study did not involve wild animals.
Field-collected samples	This study did not involve samples collected from the field.
Ethics oversight	Animal study protocols were approved by Harvard Medical School or Boston Children's Hospital's Institutional Animal Care and Use Committee.

Note that full information on the approval of the study protocol must also be provided in the manuscript.

Flow Cytometry

Plots

Confirm that:

- ☒ The axis labels state the marker and fluorochrome used (e.g. CD4-FITC).
- ☒ The axis scales are clearly visible. Include numbers along axes only for bottom left plot of group (a 'group' is an analysis of identical markers).
- ☒ All plots are contour plots with outliers or pseudocolor plots.
- ☒ A numerical value for number of cells or percentage (with statistics) is provided.

Methodology

Sample preparation	Cells were dissociated using TrypLE Expression, washed, and resuspended in FACS buffer (PBS with 10% FBS). For surface antigens, live cells were stained with fluorophore-conjugated antibodies and the viability dye CellTrace Calcein Blue, AM (Life Technologies, C34853) at 1×10^7 cells/ml for 30 minutes on ice in the dark. This viability dye is particularly important when isolating TRA-1-60(low) populations, as loss of TRA-1-60 signal could be the result of dying cell debris. For intracellular staining, cells were fixed using BD Cytofix fixation buffer (BD Biosciences, 554655) at 1×10^7 cells/ml for 20 minutes, washed with BD Perm/Wash buffer (BD Biosciences, 554723), and permeabilized in BD Perm/Wash buffer for 10 minutes, then stained with antibodies and DAPI in the dark for 30 minutes. Stained cells were washed twice with FACS buffer, filtered into a strainer-capped tube (Falcon, 352235) prior to running on flow cytometer or FACS machine.
Instrument	Samples for were analyzed on a BD LSRFortessa, and sorted on a BD FACSAria or Beckman Coulter MoFlo Astrios.
Software	BD FACSDiva and BC IntelliSort software was used during data collection and FlowJo was used for post-collection data analysis.
Cell population abundance	"Single cell" purity mode was used to ensure high purity post-sort populations.
Gating strategy	Unstained cells and compensation beads were used to inform the gating strategy.
<input checked="" type="checkbox"/> Tick this box to confirm that a figure exemplifying the gating strategy is provided in the Supplementary Information.	